Review

International Journal of Modern Physics B
Vol. 20, No. 18 (2006) 2451–2490

World Scientific
www.worldscientific.com

TWO-PHOTON NONLINEAR INTERACTION MEDIATED BY CAVITY QUANTUM ELECTRODYNAMICS SYSTEMS

KAZUKI KOSHINO

Faculty of Systems Engineering, Wakayama University,
930 Sakaedani Wakayama 640-8510, Japan
ikuzak@sys.wakayama-u.ac.jp

HAJIME ISHIHARA

Graduate School of Engineering, Osaka Prefecture University,
1-1 Gakuen-cho, Sakai, Osaka 599-8531, Japan

Received 22 May 2006

Exploiting the field-amplification effect of a cavity, the possibility of optical nonlinearity by only two photons was indicated experimentally. In the present article, we review our recent analysis of the two-photon dynamics in a cavity quantum electrodynamics (QED) system. Since a cavity-QED system is highly dispersive around its resonances, the shapes of photonic pulses are significantly deformed through interaction with the system. Thus, the present analysis is based on a formalism beyond single-mode approximations. The external photon field is treated rigorously as a continuum, which enables us to handle the two-photon wavefunction in the space representation. The degree of optical nonlinearity in a two-photon state is quantified by comparing the output wavefunction with the *linear* output wavefunction. It is revealed that the semiclassical optical response theory can be applied for evaluation of the two-photon optical nonlinearity. The two-photon nonlinearity appears not purely as a phase shift in the output wavefunction. The degradation of the fidelity between the output wavefunction and the *linear* output wavefunction always occurs, which hinders the application of this nonlinear effect as a quantum phase gate. The optimum condition for maximizing the two-photon nonlinearity is clarified, suggesting that pulse shape control is more essential than the Q-value control of the cavity QED system.

Keywords: Two-photon nonlinearity; cavity-QED; controlled phase gate; nonlinear phase shift.

1. Introduction

Cavity quantum electrodynamics (QED) concerns the properties of optically active media (typically two-level atoms) confined within a high-Q cavity.[1–3] The cavity discretizes the photonic modes inside the cavity and separates these cavity modes from the external photon field. Thus, one can realize a well-isolated quantum system composed of atoms and cavity photons, which is weakly coupled to the external photon field that acts as a reservoir. Furthermore, the external photonic modes

can be utilized as a probe for inferring the quantum states of the nearly isolated atom-cavity system. Cavity QED systems are therefore quite suitable for fundamental tests of quantum dynamics of open systems and also for quantum-state engineering utilizing the internal dynamics of the atom-cavity system.[4–12]

When photons are inputted into the cavity from the external space, these input photons are usually reflected by one of the mirrors constituting the cavity (the isolation effect). However, the role of the cavity is not restricted to isolation of the internal system. If the energy of the input photon is close to one of the resonance frequencies of the internal atom-cavity system, the photon can enter the cavity. Furthermore, the field intensity per photon is drastically enhanced inside the cavity, compared to that for free photons. Namely, the cavity can work as an amplifier for resonant input photons. Conventionally, it has been supposed that strong fields are indispensable for the induction of significant nonlinear optical effects.[13–15] However, by placing nonlinear optical media inside of a cavity and utilizing this field-amplification effect, considerable nonlinear effects can be expected, even by weak input fields. Actually, through an experiment using a two-level atom as an nonlinear optical agent, Turchette *et al.* indicated optical nonlinearity sensitive to individual photons,[16,17] which is extremely valuable in quantum information processing.[18] Together with rapid improvements in photon generation technology,[19–24] induction of optical nonlinear effects by only two photons is one of the main goals in current quantum control technology.

In the present article, we theoretically analyze the nonlinear dynamics of two photons mediated by cavity-QED systems. Since a two-photon state does not belong to classical (coherent) states, theoretical analysis of two-photon dynamics requires a fully quantum mechanical framework, in which not only the optical media but also the photon field is quantized. In the field of quantum optics,[25–28] nonlinear interaction among several photonic modes has been briskly discussed, employing a phenomenological interaction Hamiltonian based on the single-mode approximation.[29–31] The implicit assumption behind the single-mode approximation is that the spatial shapes of photonic pulses are unchanged during the interaction with the optical media, and therefore the optical media are almost dispersionless around the energies of the input photons. These assumptions can be justified when the input photons are off-resonant with respect to the optical media. However, our interest here lies in the cases in which the input photons are close to the resonance of the optical system in order to make maximum use of the strong nonlinearity around the resonance. Then, the photonic pulse shapes are expected to be significantly deformed so that the single-mode approximation cannot be applied. Thus, the present analysis is based on a formalism in which the multi-mode nature of the free-space photon field is rigorously taken into account.[32–36] This formalism allows us to handle the full information on the input and output photons, namely, the spatial wavefunction of photons.

The present article is organized as follows. In Sec. 2, we present the Hamiltonian for the cavity-QED system including the external photon field. In Sec. 3, we discuss

the optical response of the cavity-QED system when classical light fields (coherent states) are inputted. In Sec. 4, we examine how the input two-photon wavefunction is transformed through the interaction with the cavity-QED system, and evaluate the optical nonlinearity appearing in the output two-photon wavefunction. Finally, a summary is presented in Sec. 5.

2. Cavity-QED System

In this section, we present a theoretical model for a cavity-QED system and discuss its basic properties. The model system discussed in the present study is schematically illustrated in Fig. 1. A one-sided cavity is formed by two spherical mirrors. The mirror on the right is weakly transmissive and allows interaction between cavity photons and external photons. As an optically active medium, a single two-level system (hereinafter referred to as an "atom") is placed inside of the cavity. Our main interest is how the input photons are transformed after interaction with this cavity-QED system.

In order to theoretically analyze this problem, the following two points should be kept in mind: (i) A cavity-QED system is a typical open quantum system, exposed to two kinds of photonic continua, noncavity modes and the input/output field, as illustrated in Fig. 1. These continua should be treated as active mechanical degrees of freedom in order to analyze the quantum states of input/output photons. (ii) When the energies of input photons are close to the resonance of the system, the shapes of the photonic pulses are largely deformed in the output, since the system is highly dispersive around the resonance. Hence, the single-mode approximation is inadequate in this frequency region. The above two points are naturally resolved by the multimode treatment for the photonic continua, as is done in the following.

2.1. *Hamiltonian*

Here, we present the Hamiltonian for the case in which a single two-level atom is placed inside of a cavity. The system is composed of the following four parts:

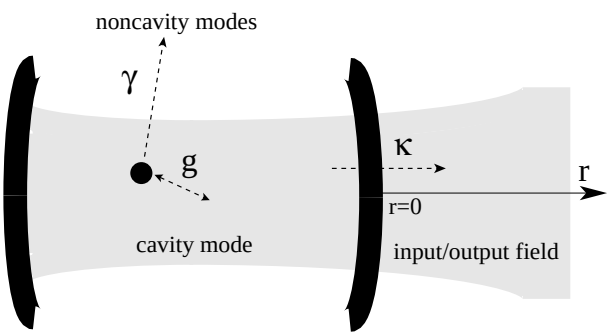

Fig. 1. Schematic illustration of a cavity-QED system composed of a two-level atom and a cavity. The meanings of the parameters are noted in Table 1.

Table 1. Meanings of the principal parameters of a cavity-QED system.

Parameter	Meaning
$\omega_{\rm a}$	Transition frequency of the two-level atom
$\omega_{\rm c}$	Resonance frequency of the cavity mode
g	Coupling between the atom and the cavity mode
κ	Escape rate of the cavity photon into the external field
γ	Atomic spontaneous emission rate into noncavity modes
$\tilde{\omega}_{\rm a}(\equiv \omega_{\rm a} - i\gamma/2)$	Complex frequency of the two-level atom
$\tilde{\omega}_{\rm c}(\equiv \omega_{\rm c} - i\kappa/2)$	Complex frequency of the cavity mode

a two-level atom, a cavity mode, the input/output field, and non-cavity modes. The annihilation operators for these elements are denoted by s, c, b_k, and d_k, respectively, where k is a continuous label representing the photonic wavenumber. The Hamiltonian for the whole system is given by

$$\mathcal{H} = \mathcal{H}_{\rm sys} + \mathcal{H}_{\rm ce} + \mathcal{H}_{\rm an}\,, \tag{1}$$

$$\mathcal{H}_{\rm sys} = \omega_{\rm a} s^\dagger s + \omega_{\rm c} c^\dagger c + g(s^\dagger c + c^\dagger s)\,, \tag{2}$$

$$\mathcal{H}_{\rm ce} = \int dk \left[k b_k^\dagger b_k + \sqrt{\frac{\kappa}{2\pi}}(c^\dagger b_k + b_k^\dagger c)\right], \tag{3}$$

$$\mathcal{H}_{\rm an} = \int dk \left[k d_k^\dagger d_k + \sqrt{\frac{\gamma}{2\pi}}(s^\dagger d_k + d_k^\dagger s)\right], \tag{4}$$

where $\mathcal{H}_{\rm sys}$ is called the Jaynes–Cummings Hamiltonian[37] and describes a completely isolated atom-cavity system, $\mathcal{H}_{\rm ce}$ describes the interaction between the cavity mode and the input/output field, and $\mathcal{H}_{\rm an}$ describes the atomic radiative dissipation to noncavity modes. The meanings of the parameters ($\omega_{\rm a}$, $\omega_{\rm c}$, g, κ and γ) are summarized in Table 1. Unless specified, $\omega_{\rm a} = \omega_{\rm c}$ is assumed in the following. Note that s is a Pauli operator, whereas c, b_k and d_k are bosonic operators. The commutators are given by

$$[s, s^\dagger] = 1 - 2s^\dagger s\,, \tag{5}$$

$$[c, c^\dagger] = 1\,, \tag{6}$$

$$[b_k, b_{k'}^\dagger] = \delta(k - k')\,, \tag{7}$$

$$[d_k, d_{k'}^\dagger] = \delta(k - k')\,. \tag{8}$$

The origin of nonlinearity in this system is attributed solely to the saturation effect of the atom, i.e. deviation from the bosonic operator in Eq. (5).

As observed in Fig. 1, the input and output fields exist only in the $r > 0$ region; the input field propagates in the negative direction whereas the output field

propagates in the positive direction. However, it is convenient to treat the input field as if it had propagated in the positive direction in the $r < 0$ region.[38] Adopting this convention, the real-space representation of the input/output field is given by

$$\tilde{b}_r = \frac{1}{\sqrt{2\pi}} \int dk e^{ikr} b_k \,, \tag{9}$$

the commutator of which is given by $[\tilde{b}_r, \tilde{b}^\dagger_{r'}] = \delta(r - r')$. Similarly, the real-space representation of the noncavity modes can be formally defined as

$$\tilde{d}_r = \frac{1}{\sqrt{2\pi}} \int dk e^{ikr} d_k \,, \tag{10}$$

the commutator of which is given by $[\tilde{d}_r, \tilde{d}^\dagger_{r'}] = \delta(r - r')$.

There are two observations regarding this Hamiltonian. (i) The transverse profile of the input/output field is determined by the radiation pattern from the cavity mode.[39,40] Thus, the input/output field is treated one-dimensionally. (ii) In $\mathcal{H}_{\rm ce}$ ($\mathcal{H}_{\rm an}$), the coupling constant between c and b_k (s and d_k) is approximated to be independent of the photonic energy k. This flat-band approximation is equivalent to the Markov approximation. Under this approximation, the decay of the cavity mode into the output field occurs purely exponentially.[41]

2.2. *Complex eigenfrequencies*

Let us discuss the eigenenergies of the atom-cavity system in an intuitive manner. The role of $\mathcal{H}_{\rm ce}$ ($\mathcal{H}_{\rm an}$) in Eq. (1) is to make the cavity mode (atomic excitation) decay with a rate of κ (γ). Adopting these dissipative effects as the imaginary parts of frequencies, we obtain a *phenomenological* Hamiltonian for the atom-cavity system as follows:

$$\mathcal{H}^{\rm ph}_{\rm sys} = \tilde{\omega}_{\rm a} s^\dagger s + \tilde{\omega}_{\rm c} c^\dagger c + g(s^\dagger c + c^\dagger s) \,, \tag{11}$$

where $\tilde{\omega}_{\rm a} (= \omega_{\rm a} - i\gamma/2)$ and $\tilde{\omega}_{\rm c} (= \omega_{\rm c} - i\kappa/2)$ are the complex frequencies for the atom and cavity mode.

Since this Hamiltonian conserves the number of total quanta, $s^\dagger s + c^\dagger c$, the Hilbert space can be divided according to the number of quanta. The one-quantum space is spanned by $s^\dagger|0\rangle$ and $c^\dagger|0\rangle$. The complex eigenenergies $\tilde{\omega}_1$ and $\tilde{\omega}_2$ in the one-quantum space are defined by

$$(z - \tilde{\omega}_{\rm a})(z - \tilde{\omega}_{\rm c}) - g^2 = (z - \tilde{\omega}_1)(z - \tilde{\omega}_2) \,. \tag{12}$$

In the two-quanta space spanned by $s^\dagger c^\dagger|0\rangle$ and $2^{-1/2} c^\dagger c^\dagger|0\rangle$, the complex eigenenergies $\tilde{\nu}_1$ and $\tilde{\nu}_2$ are defined by

$$(z - \tilde{\omega}_{\rm a} - \tilde{\omega}_{\rm c})(z - 2\tilde{\omega}_{\rm c}) - 2g^2 = (z - \tilde{\nu}_1)(z - \tilde{\nu}_2) \,. \tag{13}$$

Note that all of $\tilde{\omega}_1$, $\tilde{\omega}_2$, $\tilde{\nu}_1$ and $\tilde{\nu}_2$ lie in the lower half plane. Interestingly, these complex eigenfrequencies often appear during rigorous quantum mechanical calculations based on Eq. (1).

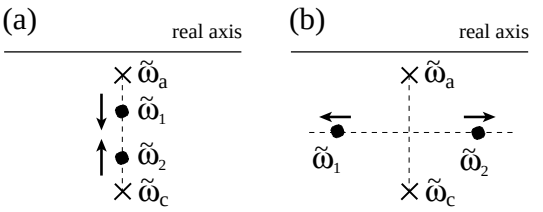

Fig. 2. Locations of $\tilde{\omega}_1$ and $\tilde{\omega}_2$ on the complex plane for (a) the weak-coupling case and (b) the strong coupling case. $\gamma < \kappa$ is assumed in this figure but is not necessary. The arrows indicate the directions into which $\tilde{\omega}_1$ and $\tilde{\omega}_2$ move as the coupling g is increased.

2.2.1. *Weak coupling and strong coupling*

Here, we investigate how $\tilde{\omega}_1$ and $\tilde{\omega}_2$ behave as functions of g. Assuming $\omega_a = \omega_c$, they are given by Eq. (12) as

$$\tilde{\omega}_{1,2} = \omega_c - i\,\frac{\kappa+\gamma}{4} \pm \sqrt{g^2 - \left(\frac{\kappa-\gamma}{4}\right)^2}\,. \tag{14}$$

In the weak-coupling case satisfying $g < |\kappa - \gamma|/4$, only the imaginary parts are modified by the atom-cavity coupling g, as shown in Fig. 2(a). In this case, the atom and cavity are regarded as essentially independent optical agents. The effect of g appears as the modification of the decay rates of the atom and cavity.

On the other hand, this simple picture breaks down in the strong-coupling case of $g > |\kappa-\gamma|/4$, where the real parts of the eigenenergies split, as shown in Fig. 2(b). In this regime, the internal dynamics of the isolated atom-cavity system becomes important; the atom and the cavity mode interchange the energy quanta during the decay, leading to a phenomenon called the collapse and revival.

2.3. *Coupling between the atom and the photon field*

2.3.1. *Quasi-cavity continuum*

In the Hamiltonian of Eq. (1), the atom is coupled via the cavity mode to the continuum of the input/output field. By diagonalizing the relevant part ($\omega_c c^\dagger c + \mathcal{H}_{ce}$), c and b_k can be recast into a single continuum, denoted by C_k and referred to as the quasi-cavity continuum. Applying the Fano method,[42] C_k is given by

$$C_k = \eta(k)c + \int dq\zeta(k,q)b_q\,, \tag{15}$$

$$\eta(k) = \sqrt{\frac{\kappa}{2\pi}}\,\frac{1}{k-\tilde{\omega}_c}\,, \tag{16}$$

$$\zeta(k,q) = \frac{\kappa}{2\pi}\,\frac{1}{(k-\tilde{\omega}_c)(k-q+i\delta)} + \delta(k-q)\,. \tag{17}$$

It is orthonormalized as $[C_k, C_{k'}^\dagger] = \delta(k - k')$. Inversely, the original operators are given by $c = \int dk\eta^*(k)C_k$ and $b_q = \int dk\zeta^*(k,q)C_k$. The function $\eta(k)$ has meaning as the dressed Green's function for the cavity photon (see Appendix C). In terms of C_k, the real-space representation $\tilde{b}_r$ of the input/output field is given by

$$\tilde{b}_r = \begin{cases} (2\pi)^{-1/2} \int dk e^{ikr} \dfrac{\eta^*(k)}{\eta(k)} C_k & (\text{input field}, r < 0) \\ (2\pi)^{-1/2} \int dk e^{ikr} C_k & (\text{output field}, r > 0)\,. \end{cases} \tag{18}$$

2.3.2. *Form factors of the atom-photon interaction*

Using the quasi-cavity operator C_k, the original Hamiltonian is recast into the following form:

$$\mathcal{H} = \omega_{\rm a} s^\dagger s + \int dk[kC_k^\dagger C_k + (g\eta^*(k)s^\dagger C_k + \text{H.c.})] + \mathcal{H}_{\rm an}\,. \tag{19}$$

Thus, the atom is coupled to two kinds of photonic continua: the quasi-cavity continuum (C_k) and the noncavity modes (d_k). The squared coupling constants to these continua, referred to as the form factors and denoted by $|\xi_{\rm c}(k)|^2$ and $|\xi_{\rm n}(k)|^2$, are given by

$$|\xi_{\rm c}(k)|^2 = |g\eta(k)|^2 = \frac{g^2\kappa}{2\pi} \frac{1}{|k - \tilde{\omega}_{\rm c}|^2}\,, \tag{20}$$

$$|\xi_{\rm n}(k)|^2 = \frac{\gamma}{2\pi}\,. \tag{21}$$

$|\xi_{\rm c}(k)|^2$ is a Lorentzian with half-width κ and area g^2. The overall form factor $|\xi_{\rm t}(k)|^2$ is defined by

$$|\xi_{\rm t}(k)|^2 = |\xi_{\rm c}(k)|^2 + |\xi_{\rm n}(k)|^2\,. \tag{22}$$

The shapes of these form factors are shown in Fig. 3(a).

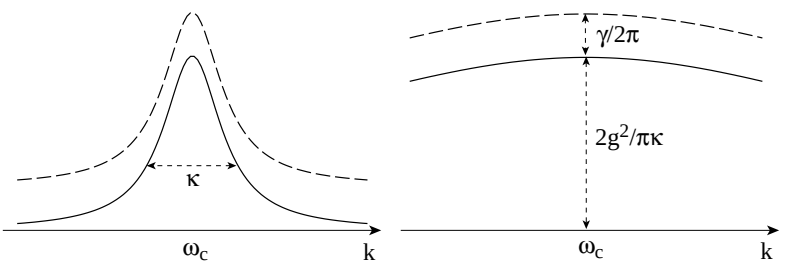

Fig. 3. (a) Form factors for the Hamiltonian of Eq. (19). $|\xi_{\rm c}(k)|^2$ and $|\xi_{\rm t}(k)|^2$ are plotted by the solid and broken lines, respectively. (b) Form factors for a one-dimensional atom.

2.3.3. *One-dimensional atom*

In the limit of extremely weak coupling satisfying $\kappa \gg g$, $|\xi_{\rm c}(k)|^2$ can be regarded as an almost constant function ($\sim 2g^2/\pi\kappa$) around the resonance frequency, as shown in Fig. 3(b). Furthermore, if $g^2/\kappa \gg \gamma$ is satisfied, the atom is coupled principally to the quasi-cavity continuum. In this case, most of the emission from the atom is directed to the one-dimensional output field (the leak pattern from the cavity). Hence, the system is called a one-dimensional atom[16,17] in this parameter region ($\kappa \gg g^2/\kappa \gg \gamma$). The parameters that characterize a one-dimensional atom are the overall coupling Γ and the fraction β, which are given by

$$\Gamma = \gamma + 4g^2/\kappa\,, \tag{23}$$

$$\beta = (4g^2/\kappa)/\Gamma\,. \tag{24}$$

2.4. *Cavity-QED parameters for a planar cavity*

When a cavity is formed by two spherical mirrors as in Fig. 1, the geometry of the cavity uniquely specifies the spatial form of the privileged cavity mode.[39,40] g and κ are determined by the geometrical parameters (atomic position, cavity length, curvature of the mirrors, etc.), while κ is determined by the transmissivity of the mirrors. In contrast, for the case of a planar cavity, one can choose the lateral profile of the input beam more arbitrarily. The input beam profile is then relevant for determination of the *effective* cavity mode function and, therefore, of the cavity-QED parameters, g, κ and γ (see Sec. 2.4.1). Here, we present a method by which to determine these parameters for the case of planar cavity on the basis of a three-dimensional formalism.[43]

The configuration of the system considered is illustrated in Fig. 4. A planar one-sided cavity is formed by a perfect mirror at $z = -l$ and a leaky mirror with transmissivity T at $z = 0$. Therefore, the cutoff frequency $\omega_{\rm cut}$ for the intra-cavity field is given by $\omega_{\rm cut} = \pi/l$. A two-level atom with resonance frequency $\omega_{\rm a}$ and

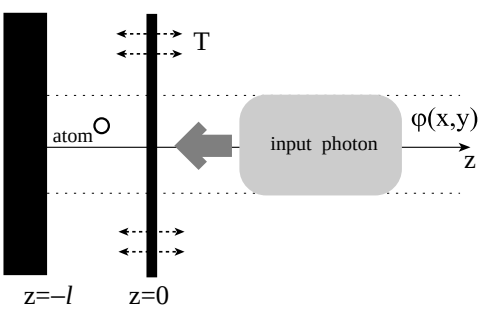

Fig. 4. Configuration of a planar cavity-QED system. The left mirror at $z = -l$ is perfect, whereas the right mirror at $z = 0$ has a small transmissivity T. The atom is placed at $\boldsymbol{R} = (X, Y, Z)$, where $-l < Z < 0$. The lateral profile of the input beam is assumed to be z-independent.

transition dipole $\wp$ is placed at $\boldsymbol{R} = (X, Y, Z)$. We consider the case of $\omega_{\rm a} \simeq \omega_{\rm cut}$, where only the lowest subband of the intra-cavity field is relevant. The input beam propagates along the z-axis with a fixed lateral profile, assuming that the beam diameter is well above the diffraction limit.

2.4.1. *Intuitive consideration*

Before proceeding to rigorous analysis, we estimate the parameters g and κ intuitively as follows. The lateral profile of the input beam is denoted by $\varphi(x, y)$, which is normalized as $\int dxdy|\varphi(x, y)|^2 = 1$. Then, the normalized cavity-mode function is given by $f_{\rm cav}(\boldsymbol{r}) = (2\omega_{\rm cut}/\pi)^{1/2} \sin(\omega_{\rm cut} z) \times \varphi(x, y)$. Therefore, the atom-cavity coupling g is expected to be

$$g_{\rm est} = \frac{\wp\omega_{\rm a}}{\sqrt{2\omega_{\rm cut}}} f_{\rm cav}(\boldsymbol{R}) = \frac{\wp\omega_{\rm a}}{\sqrt{\pi}} \sin(\omega_{\rm cut} Z)\varphi(X, Y)\,. \tag{25}$$

The escape rate of the cavity photon is expected to be

$$\kappa_{\rm est} = T/2l = T\omega_{\rm cut}/2\pi\,. \tag{26}$$

The validity of these estimations is examined in the following part of this section.

2.4.2. *Three-dimensional Hamiltonian*

The system is composed of three parts: the atom, the intra-cavity field ($-l < z < 0$), and the external field ($0 < z$). Because k_z is fixed at $\omega_{\rm cut}$ inside the cavity, the intra-cavity field is labeled by a two-dimensional in-plane wavevector $\vec{k} = (k_x, k_y)$, whereas the external field is labeled three-dimensionally by $\boldsymbol{k} = (k_x, k_y, k_z)$. The Hamiltonian is given by

$$\begin{aligned}\mathcal{H}_{\rm planar} = \omega_{\rm a} s^\dagger s + \int d^2\vec{k}[\omega_{\vec{k}} c_{\vec{k}}^\dagger c_{\vec{k}} + (\lambda_{\vec{k}} s^\dagger c_{\vec{k}} + {\rm H.c.})] \\ + \int d^3\boldsymbol{k} \left[\omega_{\boldsymbol{k}} b_{\boldsymbol{k}}^\dagger b_{\boldsymbol{k}} + \left(\frac{c_{\vec{k}}^\dagger b_{\boldsymbol{k}}}{\sqrt{2\pi\tau_{\vec{k}}}} + {\rm H.c.}\right)\right],\end{aligned} \tag{27}$$

where $c_{\vec{k}}$ and $b_{\boldsymbol{k}}$ are the annihilation operators for the intra-cavity field and the external field, normalized as $[c_{\vec{k}}, c_{\vec{k}'}^\dagger] = \delta^2(\vec{k} - \vec{k}')$ and $[b_{\boldsymbol{k}}, b_{\boldsymbol{k}'}^\dagger] = \delta^3(\boldsymbol{k} - \boldsymbol{k}')$. $\omega_{\vec{k}}$ and $\omega_{\boldsymbol{k}}$ denote the frequencies for $c_{\vec{k}}$ and $b_{\boldsymbol{k}}$, which are given by $\omega_{\vec{k}} = (\omega_{\rm cut}^2 + |\vec{k}|^2)^{1/2}$ and $\omega_{\boldsymbol{k}} = |\boldsymbol{k}|$. $\tau_{\vec{k}}$ denotes the lifetime of $c_{\vec{k}}$, which is given by $\tau_{\vec{k}} = 2\pi\omega_{\vec{k}}/T\omega_{\rm cut}^2$. Finally, the atom-photon coupling $\lambda_{\vec{k}}$ reads

$$\lambda_{\vec{k}} = \frac{\wp\omega_{\rm a}}{\sqrt{2\omega_{\vec{k}}}} f_{\vec{k}}(\boldsymbol{R})\,, \tag{28}$$

where $f_{\vec{k}}(\boldsymbol{r}) = \sqrt{\omega_{\rm cut}/2\pi^3} \sin(\omega_{\rm cut} z) \exp[i(k_x x + k_y y)]$ is the spatial mode function for $c_{\vec{k}}$. Note that the in-plane wave vector $\vec{k}$ is conserved during the interaction between the $c_{\vec{k}}$ and $b_{\boldsymbol{k}}$ due to the in-plane translational symmetry.

2.4.3. *Form factors*

Based on the above Hamiltonian and the lateral profile $\varphi(x, y)$ of the input beam, one can calculate the form factors, $|\xi_{\rm t}(\omega)|^2$ and $|\xi_{\rm c}(\omega)|^2$, introduced in Sec. 2.3.2. They are given by

$$|\xi_{\rm t}(\omega)|^2 = \int d^2\vec{k}|\lambda_{\vec{k}}\eta_{\vec{k}}(\omega)|^2\,, \tag{29}$$

$$|\xi_{\rm c}(\omega)|^2 = \left|\int d^2\vec{k}\lambda_{\vec{k}}\eta_{\vec{k}}(\omega)\tilde{\varphi}(\vec{k})\right|^2\,, \tag{30}$$

where $\tilde{\varphi}(\vec{k})$ is the Fourier transform of $\varphi(x, y)$, and $\eta_{\vec{k}}(\omega)$ is the dressed Green's function for $c_{\vec{k}}$, as given by

$$\eta_{\vec{k}}(\omega) = \frac{(2\pi\tau_{\vec{k}})^{-1/2}}{\omega - \omega_{\vec{k}} + i/2\tau_{\vec{k}}}\,. \tag{31}$$

These formulas are derived in Appendix A.

The overall form factor $|\xi_{\rm t}(\omega)|^2$ governs the dynamics of spontaneous decay of an excited atom. Expectedly, $|\xi_{\rm t}(\omega)|^2$ is independent of the in-plane atomic position (X, Y) and also of the input beam profile. In contrast, $|\xi_{\rm c}(\omega)|^2$ is sensitive to the location of the effective cavity mode generated by the input beam. By the Schwartz inequality, $|\xi_{\rm c}(\omega)|^2 \leq \int d^2\vec{k}|\tilde{\varphi}(\vec{k})|^2 \times \int d^2\vec{k}|\lambda_{\vec{k}}\eta_{\vec{k}}(\omega)|^2 = |\xi_{\rm t}(\omega)|^2$, in accordance with the definitions of these form factors.

The concrete forms of the form factors are shown in Fig. 5. It is assumed that the atom is placed at the center of the cavity, i.e. $\boldsymbol{R} = (0, 0, -l/2)$, and that the lateral beam profile is Gaussian with diameter $2d$, i.e. $\varphi(x, y) = (\pi d^2)^{-1/2}\exp[-(x^2 + y^2)/2d^2]$. The overall form factor $|\xi_{\rm t}(\omega)|^2$ is independent of the beam profile and is determined solely by the transmissivity. In addition, $|\xi_{\rm t}(\omega)|^2$ shows a step-like

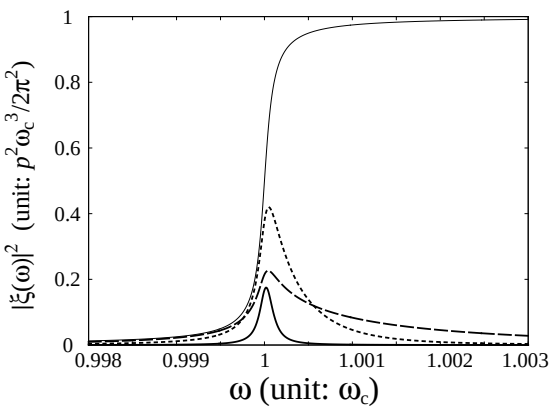

Fig. 5. Form factors for a planar cavity geometry: $|\xi_{\rm t}(\omega)|^2$ (thin line) and $|\xi_{\rm c}(\omega)|^2$ (bold lines). Transmissivity is fixed at $T = 10^{-3}$. The beam diameter is chosen at $d = 20\omega_{\rm cut}^{-1}$ (dashed line), $50\omega_{\rm cut}^{-1}$ (dotted line), and $200\omega_{\rm cut}^{-1}$ (solid line).

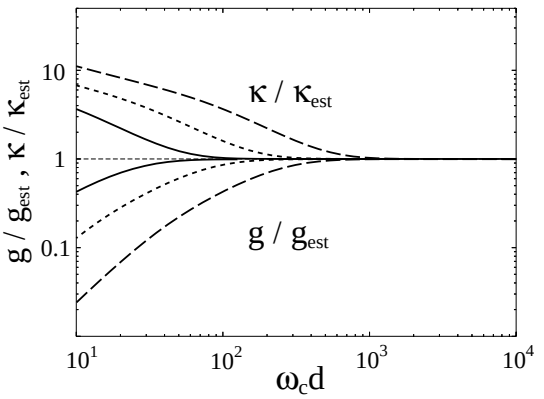

Fig. 6. Plot of $g/g_{\rm est}$ and $\kappa/\kappa_{\rm est}$ as functions of beam diameter $2d$. The transmissivities are chosen at $T = 10^{-2}$ (solid lines), $T = 10^{-3}$ (dotted lines) and $T = 10^{-4}$ (dashed lines).

behavior characteristic to the two-dimensional photon field.[44] Approximating $\tau_{\vec{k}}$ by $\tau_{\vec{0}}$ in Eq. (29), $|\xi_{\rm t}(\omega)|^2$ is obtained analytically as

$$|\xi_{\rm t}(\omega)|^2 = \frac{\wp^2\omega_{\rm cut}^3}{2\pi^2}\left[\frac{1}{2} + \frac{1}{\pi}\arctan\left(\frac{4\pi}{T\omega_{\rm cut}}(\omega - \omega_{\rm cut})\right)\right]. \tag{32}$$

On the other hand, $|\xi_{\rm c}(\omega)|^2$ is sensitive to the input beam profile. When the beam diameter is large (bold solid line in Fig. 5), $|\xi_{\rm c}(\omega)|^2$ reduces to a genuine Lorentzian, which agrees well with Eq. (20), with estimated parameters $g_{\rm est}$ and $\kappa_{\rm est}$ given by Eqs. (25) and (26). As the beam is collimated, the atom–cavity coupling is strengthened and $|\xi_{\rm c}(\omega)|^2$ becomes larger (dotted line in Fig. 5). However, $|\xi_{\rm c}(\omega)|^2$ cannot grow freely due to the upper bound imparted by the condition $|\xi_{\rm c}(\omega)|^2 \leq |\xi_{\rm t}(\omega)|^2$. This upper bound is expected to become important when d is sufficiently small to satisfy $\omega_{\rm cut}d \lesssim 4T^{-1/2}$.[a] When the beam diameter is smaller than this value, $|\xi_{\rm c}(\omega)|^2$ deviates considerably from a Lorentzian (dashed line in Fig. 5).

2.4.4. *Connection to the cavity-QED parameters*

One can determine the cavity-QED parameters from these two form factors, by comparing them with the form factors for a (g, κ, γ)-model given by Eqs. (20)–(22). Equation (20) suggests that the area and half-width of $|\xi_{\rm c}(\omega)|^2$ correspond to g^2 and κ, respectively. Figure 6 plots g and κ thus obtained as functions of the beam diameter $2d$. In the large diameter region, g and κ are in good agreement with the estimations, $g_{\rm est}$ and $\kappa_{\rm est}$. However, in the small diameter region specified by $\omega_{\rm cut}d \lesssim 4T^{-1/2}$, g and κ deviate appreciably from the estimations.

On the other hand, γ is determined from the coupling to noncavity modes, given by $|\xi_{\rm n}(\omega)|^2 = |\xi_{\rm t}(\omega)|^2 - |\xi_{\rm c}(\omega)|^2$. As observed in Fig. 5, $|\xi_{\rm n}(\omega)|^2$ is highly

[a]This condition is obtained by comparing $|\xi_{\rm t}(\omega)|^2$ [Eq. (29)] and $|\xi_{\rm c}(\omega)|^2$ [Eq. (20) with Eqs. (25) and (26)] at $\omega = \omega_{\rm cut}$.

dispersive around the cutoff energy, although such dispersion is neglected in the conventional (g, κ, γ)-model of Eq. (1). Reviving the ω-dependence, $\gamma(\omega)$ is given by $\gamma(\omega) = 2\pi(|\xi_{\rm t}(\omega)|^2 - |\xi_{\rm c}(\omega)|^2)$.

As an realistic example, we here consider the case in which the "atom" is a quantum dot with $\omega_{\rm a} = 1$ eV and a diameter of 10 nm.[b] When $T = 10^{-3}$ and $d = 50\omega_{\rm cut}^{-1} \simeq 10\ \mu$m in reference to the dotted line in Fig. 5, $g/\omega_{\rm cut} \simeq 6\times10^{-5}$ and $\kappa/\omega_{\rm cut} \simeq 4\times10^{-4}$. γ is best suppressed at $\omega \simeq 0.9998\omega_{\rm cut}$, where $\gamma/\omega_{\rm cut} \simeq 7\times10^{-7}$.

3. Optical Response Against Classical Light

In this section, we investigate the optical response of cavity-QED systems when classical light fields are inputted. Since the outputs from conventional lasers are classical regardless of whether they are pulsed or continuous, the analysis presented in this section covers most experiments using conventional laser fields. Furthermore, as will be revealed later (see Sec. 4.3), the linear and nonlinear responses to a pulsed classical light are closely related to the nonlinear interaction between two photons.

The analysis in this section is restricted for simplicity to the single-atom case, the Hamiltonian of which has been presented in Sec. 2.1. Extension to more complicated situations (e.g. excitonic systems inside of a cavity) is straightforward, as shown in Appendix B.

3.1. *Basic equations of motion*

3.1.1. *Initial state*

As the initial moment t_0, we choose an arbitrary moment at which the input field has not arrived at the cavity. Denoting the field amplitude at t_0 by $f_{\rm in}(r)$, which is nonzero only in the $r < 0$ region, the initial quantum state is given by

$$|\Phi_{\rm in}\rangle = \exp\left(-\int dr|f_{\rm in}(r)|^2/2\right)\exp\left(\int dr f_{\rm in}(r)\tilde{b}_r^\dagger\right)|0\rangle\,, \tag{33}$$

where $\tilde{b}_r$ is the real-space representation of the input/output field, defined in Eq. (9). As usual, the other parts of the system (the atom, the cavity mode, and the output field) are assumed to be in the ground state initially. In this section, we will investigate the quantum time evolution from the above initial state, determined by the Hamiltonian of Eq. (1).

3.1.2. *Heisenberg equations*

Cavity-QED systems are typical open quantum systems, in which relevant mechanical degrees of freedom (atom and cavity mode) are coupled to heat baths

[b]The diameter a of a quantum dot roughly determines the transition dipole moment $\wp$. Denoting the electronic charge by q, the dipole moment is given by $\wp \simeq qa$.

(input/output field and noncavity modes). When discussing open systems, the mechanical degrees of freedom for the heat baths are often eliminated. However, in the present problem, the continuum b_k (the input/output field) should not be eliminated because we are interested in the input and output photons. Here, we present a method to handle the photonic continua as active mechanical degrees of freedom, that is known as the input-output formalism.[27,28]

The Heisenberg equation for b_k is given, using Eq. (3), by

$$\dot{b}_k = -ikb_k - i\sqrt{\kappa/2\pi}\, c\,. \tag{34}$$

Denoting the initial and final moments by t_0 and t_1, the operator at time τ ($t_0 < \tau < t_1$) is represented in two ways:

$$b_k(\tau) = b_k(t_0)e^{-ik(\tau-t_0)} - i\sqrt{\frac{\kappa}{2\pi}}\int_{t_0}^{\tau} d\tau' c(\tau')e^{-ik(\tau-\tau')} \tag{35}$$

$$= b_k(t_1)e^{-ik(\tau-t_1)} + i\sqrt{\frac{\kappa}{2\pi}}\int_{\tau}^{t_1} d\tau' c(\tau')e^{-ik(\tau-\tau')}\,. \tag{36}$$

Using the above two forms of $b_k(\tau)$, $\int dk b_k(\tau)$ is recast into the following two forms:

$$\int dk b_k(\tau) = \sqrt{2\pi}\,\tilde{b}_{t_0-\tau}(t_0) - i\sqrt{\frac{\pi\kappa}{2}}c(\tau) \tag{37}$$

$$= \sqrt{2\pi}\,\tilde{b}_{t_1-\tau}(t_1) + i\sqrt{\frac{\pi\kappa}{2}}c(\tau)\,, \tag{38}$$

with the help of Eq. (9). Equating the right hand sides and introducing new labels $r(= t_1 - \tau)$ and $t(= t_1)$, we obtain the input-output relation, as given by

$$\tilde{b}_r(t) = \tilde{b}_{r-t+t_0}(t_0) - i\sqrt{\kappa}\, c(t-r)\,, \tag{39}$$

where $0 < r < t - t_0$. Thus, the output field operator at time t is expressed in terms of the input field operator at t_0 and the cavity-mode operator at $t - r$. Similarly, the input-output relation for $\tilde{d}_r$ is given by

$$\tilde{d}_r(t) = \tilde{d}_{r-t+t_0}(t_0) - i\sqrt{\gamma}\, s(t-r)\,. \tag{40}$$

The Heisenberg equations for the atomic operator s and the cavity-mode operator c are obtained from Eqs. (1)–(4). Choosing $\omega_{\rm a}(= \omega_{\rm c})$ as the origin of frequency and using Eq. (37) and its counterpart for $\int dk d_{jk}$, they are given by

$$\frac{d}{dt}s = -\frac{\gamma}{2}s - ig(1-2s^\dagger s)c - i\sqrt{\gamma}(1-2s^\dagger s)\tilde{d}_{t_0-t}(t_0)\,, \tag{41}$$

$$\frac{d}{dt}c = -\frac{\kappa}{2}c - igs - i\sqrt{\kappa}\,\tilde{b}_{t_0-t}(t_0)\,. \tag{42}$$

Equations (41) and (42), together with Eqs. (39) and (40), are the basic equations in the analysis in this section.

3.1.3. *Semiclassical equations*

Since we are working in the Heisenberg representation, the mean value of an operator A at time t is given by

$$\langle A\rangle = \langle\Phi_{\rm in}|A(t)|\Phi_{\rm in}\rangle\,, \tag{43}$$

where $|\Phi_{\rm in}\rangle$ is the initial state vector given by Eq. (33). Recall here that $|\Phi_{\rm in}\rangle$ is in the coherent state and therefore

$$\tilde{b}_r(t_0)|\Phi_{\rm in}\rangle = f_{\rm in}(r)|\Phi_{\rm in}\rangle\,, \tag{44}$$

$$\tilde{d}_r(t_0)|\Phi_{\rm in}\rangle = 0\,. \tag{45}$$

These equations imply that the input field operator $\tilde{b}_r(t_0)$ can be replaced with a c-number $f_{\rm in}(r)$, and that the terms containing $\tilde{d}_r(t_0)$ vanish.[c] The equations of motion for $\langle s\rangle$ and $\langle c\rangle$ are given by

$$\frac{d}{dt}\langle s\rangle = -\frac{\gamma}{2}\langle s\rangle - ig(\langle c\rangle - 2\langle s^\dagger sc\rangle)\,, \tag{46}$$

$$\frac{d}{dt}\langle c\rangle = -\frac{\kappa}{2}\langle c\rangle - ig\langle s\rangle - i\sqrt{\kappa}f_{\rm in}(t_0-t)\,. \tag{47}$$

The input field operators are now reduced to classical field amplitudes. Namely, *semiclassical* equations of motion for the atom-cavity system are obtained. The above simultaneous equations of motion are not closed within $\langle s\rangle$ and $\langle c\rangle$, but contain a higher-order quantity, $\langle s^\dagger sc\rangle$. The handling of such higher-order terms by the perturbation method is discussed in Sec. 3.3 and Appendix B. Finally, the amplitude $f_{\rm out}(r,t)$ of the output field is given, using Eqs. (39), by

$$f_{\rm out}(r,t) \equiv \langle\tilde{b}_r(t)\rangle = f_{\rm in}(r-t+t_0) - i\sqrt{\kappa}\langle c(t-r)\rangle\,. \tag{48}$$

3.2. *Example: One-dimensional atom*

3.2.1. *Basic equations*

As has been observed, the equation of motion for the atom-cavity system are not closed in general. However, the equations of motion become closed for the case of a one-dimensional atom (Sec. 2.3.3), which is realized when $\kappa \gg g^2/\kappa \gg \gamma$. Since damping of the cavity mode occurs much faster than other processes ($\kappa \gg g, \gamma$), Eq. (42) can be solved adiabatically. The cavity operator c is given by

$$c = -\frac{2ig}{\kappa}s - \frac{2i}{\sqrt{\kappa}}\tilde{b}_{t_0-t}(t_0)\,. \tag{49}$$

[c]The direct meaning of Eqs. (44) and (45) is that such replacements are possible only when $\tilde{b}_r(t_0)$ or $\tilde{d}_r(t_0)$ appears in the rightmost position in the term. However, this restriction is unnecessary. For example, a term $\langle s^\dagger\tilde{d}_{t_0-t}(t_0)c\rangle$ appears in the equation of motion for $\langle s^\dagger sc\rangle$. However, $\tilde{b}_{t_0-t}(t_0)$ and $\tilde{d}_{t_0-t}(t_0)$ are composed of only annihilation operators at time t, as can be observed in Eq. (37). Therefore, $\tilde{b}_{t_0-t}(t_0)$ and $\tilde{d}_{t_0-t}(t_0)$ are commutable with any annihilation operator at t and so can always be transferred to the rightmost position.

Substituting Eq. (49) into Eq. (41), we obtain

$$\frac{d}{dt}s = -\frac{\Gamma}{2}s - \sqrt{\beta\Gamma}\,(1-2s^\dagger s)\tilde{b}_{t_0-t}(t_0) - i\sqrt{(1-\beta)\Gamma}\,(1-2s^\dagger s)\tilde{d}_{t_0-t}(t_0)\,, \quad (50)$$

where Γ and β denote the overall decay rate and the fraction to the quasi-cavity continuum, defined by Eqs. (23) and (24), respectively. From Eq. (50), the equations of motion for $\langle s\rangle$ and $\langle s^\dagger s\rangle$ are derived as follows:

$$\frac{d}{dt}\langle s\rangle = -\frac{\Gamma}{2}\langle s\rangle - \sqrt{\beta\Gamma}\,(1-2\langle s^\dagger s\rangle) f_{\rm in}(t_0-t)\,, \quad (51)$$

$$\frac{d}{dt}\langle s^\dagger s\rangle = -\Gamma\langle s^\dagger s\rangle - \sqrt{\beta\Gamma}\,(f^*_{\rm in}(t_0-t)\langle s\rangle + {\rm c.c.})\,. \quad (52)$$

Thus, the above equations are closed within $\langle s\rangle$ and $\langle s^\dagger s\rangle$. The amplitude of the output field is given, from Eqs. (48) and (49), by

$$f_{\rm out}(r,t) = -f_{\rm in}(r-t+t_0) - \sqrt{\beta\Gamma}\langle s(t-r)\rangle\,. \quad (53)$$

3.2.2. *Stationary solution*

We here consider the simplest case in which the input field is monochromatic as $f_{\rm in}(r) = Ee^{ikr}$, where E is the amplitude and k is the frequency measured from $\omega_{\rm a}$. Since $f_{\rm in}(t_0-t)$ depends on time as $f_{\rm in}(t_0-t)\sim e^{-ikt}$, $\langle s\rangle$ depends on time as $\langle s\rangle \sim e^{-ikt}$ and $\langle s^\dagger s\rangle$ becomes independent of time in the stationary state. The stationary solutions of Eqs. (51) and (52) are given by[45]

$$\langle s\rangle = -\frac{\sqrt{\beta\Gamma}\,(\Gamma/2+ik)}{|\Gamma/2-ik|^2+2\beta\Gamma|E|^2}Ee^{ik(t_0-t)}\,, \quad (54)$$

$$\langle s^\dagger s\rangle = \frac{\beta\Gamma|E|^2}{|\Gamma/2-ik|^2+2\beta\Gamma|E|^2}\,. \quad (55)$$

The mean intracavity photon number $\langle c^\dagger c\rangle$ and the output amplitude $f_{\rm out}(r,t)$ are given by

$$\kappa\langle c^\dagger c\rangle = \left(4 - \frac{\beta(2-\beta)\Gamma^2}{|\Gamma/2-ik|^2+2\beta\Gamma|E|^2}\right)|E|^2\,, \quad (56)$$

$$f_{\rm out}(r,t) = \mathcal{A}\times f_{\rm in}(r-t+t_0)\,, \quad (57)$$

where the factor $\mathcal{A}$ is given by

$$\mathcal{A} = \frac{\beta\Gamma(\Gamma/2+ik)}{|\Gamma/2-ik|^2+2\beta\Gamma|E|^2} - 1\,. \quad (58)$$

The nonlinear effects have already been included in the above equations, for example, as the $2\beta\Gamma|E|^2$ term in the denominator of Eq. (54). Equation (57) shows that the output field acquires a factor $\mathcal{A}$ as a result of the interaction with a one-dimensional atom.

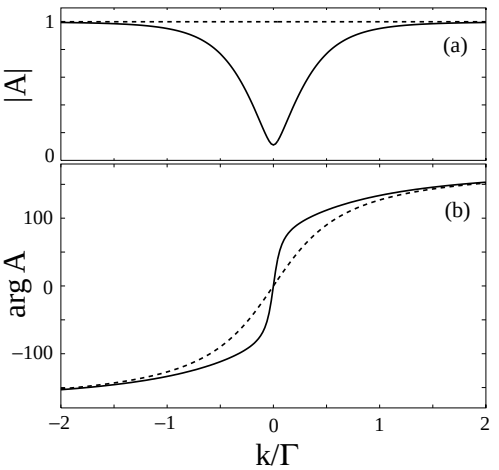

Fig. 7. Modulus and phase of $\mathcal{A}$ as functions of the detuning k of the input field. It is assumed that the atom-cavity system is dissipationless (γ=0, $\beta = 1$). The linear case ($|E|^2/\Gamma \to 0$) is plotted by the dotted lines, whereas the nonlinear case ($|E|^2/\Gamma = 0.1$) is plotted by the solid lines. The parameters g and κ are chosen at 20 and 80 MHz ($\Gamma = 20$ MHz), respectively.

3.2.3. *Linear and nonlinear phase shift*

In the linear limit of $|E|^2 \to 0$, the factor $\mathcal{A}$ is recast into the following form:

$$\mathcal{A}_{\rm lin} = \frac{(\beta - 1/2)\Gamma + ik}{\Gamma/2 - ik}\,. \tag{59}$$

In the dissipationless limit of $\beta \to 1$, the modulus of field amplitude is conserved, i.e. $|\mathcal{A}_{\rm lin}| = 1$. The output field suffers a *linear* phase shift θ that is determined by the following equation: $e^{i\theta} = (\Gamma/2+ik)/(\Gamma/2-ik)$. This linear phase shift is plotted in Fig. 7(b) by a dotted line as a function of the input frequency k. In contrast, when the system is dissipative ($\beta < 1$), the output field becomes attenuated as expected. The output field is in the coherent state, and the excess energy is radiated into the noncavity modes.

The nonlinear effect alters the phase and the modulus of $\mathcal{A}$, which are plotted in Fig. 7 as functions of the input energy k for the dissipationless case of $\beta = 1$. Figure 7(a) shows that the output amplitude becomes attenuated around the resonance, i.e. $|\mathcal{A}| < 1$, even in the dissipationless case.[45,46] Since the field energy must be conserved, the field energy is larger than the squared amplitude in the output port. Namely, the output field is not in a genuine coherent state.[d] In the off-resonant region, the output amplitude is almost maintained, i.e. $|\mathcal{A}| \simeq 1$, and the nonlinear effect appears principally as the phase shift. Defining the nonlinear phase shift by $\arg(\mathcal{A}) - \arg(\mathcal{A}_{\rm lin})$, the nonlinear phase shift is plotted in Fig. 8 as a function

[d]The field energy is generally larger than the squared amplitude, except for the case of a genuine coherent state.

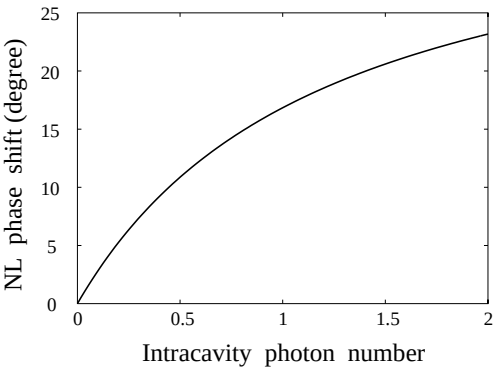

Fig. 8. Nonlinear phase shift, $\arg(\mathcal{A}) - -\arg(\mathcal{A}_{\rm lin})$, as a function of the intracavity photon number $\langle c^\dagger c\rangle$ calculated by Eq. (56). (g, κ, γ) are the same as those of Fig. 7, and the detuning of the input frequency is chosen at 30 MHz, by which $k/\Gamma = 1.5$.

of the mean intracavity photon number given by Eq. (56). Figure 8 shows that a significant nonlinear phase shift (several tens of degrees) can be expected, even by several intracavity photons. Thus, a one-dimensional atom has strong optical nonlinearity sensitive to individual photons.

3.3. *Linear and nonlinear outputs for pulsed input*

Now let us return to the general situation discussed in Sec. 3.1. In order to obtain the output field by Eq. (48), the mean amplitude $\langle c\rangle$ of the cavity field must be calculated. However, the equations of motion that determine $\langle c\rangle$ are not closed in general. (The equation of motion for $\langle s\rangle$, Eq. (46), contains a third-order quantity, $\langle s^\dagger sc\rangle$. The equations of motion for this quantity, which are obtained by combining Eqs. (41) and (42), contain further higher-order quantities.) A standard method to solve such nonlinear equations is perturbation. The equations of motion up to third-order quantities are presented in Appendix B. The linear and nonlinear components of the output field are given by $f^{(1)}_{\rm out}(r,t) = f_{\rm in}(r - t + t_0) - i\sqrt{\kappa}\langle c^{(1)}(t - r)\rangle$ and $f^{(3)}_{\rm out}(r,t) = -i\sqrt{\kappa}\langle c^{(3)}(t - r)\rangle$, where $\langle c^{(1)}\rangle$ and $\langle c^{(3)}\rangle$ denote the linear and third-order components of $\langle c\rangle$.

Figure 9 plots $f^{(1)}_{\rm out}(r,t)$ and $f^{(3)}_{\rm out}(r,t)$, where the system is in the weak coupling regime ($\kappa/g = 5$, $\gamma = 0$). A Gaussian wavepacket is assumed for the input field:

$$f_{\rm in}(r) = \left(\frac{2}{\pi d^2}\right)^{1/4} \exp[-(r/d)^2 + ikr]\,, \tag{60}$$

where d and k represent the pulse length and the central frequency, respectively. It is readily confirmed that this wavepacket is normalized as $\int dr|f_{\rm in}(r)|^2 = 1$. Namely, this is an extremely weak pulse, containing only one photon on average.

In general, due to the interaction with the optical media, the output pulse is deformed and delayed in comparison with the input pulse. In the off-resonant

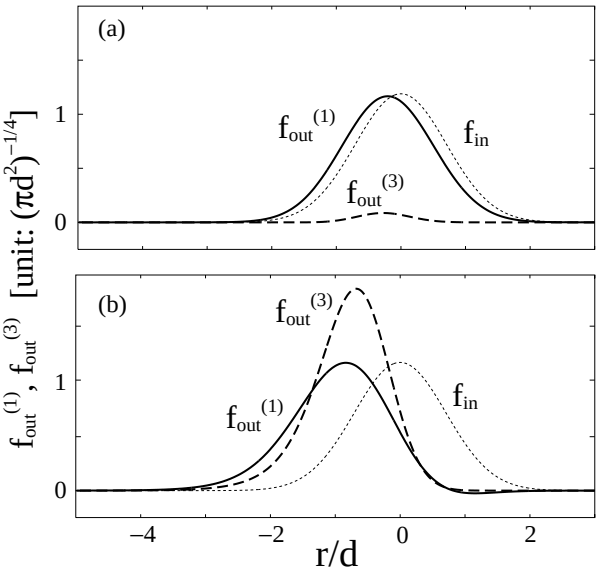

Fig. 9. Envelopes for the input and output pulses observed from a moving coordinate with the light velocity: $f_{\rm in}$ (thin dotted line), $f_{\rm out}^{(1)}$ (solid line), and $f_{\rm out}^{(3)}$ (dashed line). The system parameters are $\kappa/g = 5$ and $\gamma = 0$, and the pulse length is chosen at $d = \kappa/g^2$. The input field is off-resonant ($k/g = 1.5$) in (a), and resonant ($k = 0$) in (b).

case [see Fig. 9(a)], this delay is slight and the pulse shape is kept almost unchanged. The third-order component $f_{\rm out}^{(3)}$ is much smaller than the linear component $f_{\rm out}^{(1)}$. Contrarily, in the resonant case [see Fig. 9(b)], the output pulse is delayed and deformed significantly. Furthermore, it should be remarked that the third-order component $f_{\rm out}^{(3)}$ has an amplitude that is comparable to the linear component $f_{\rm out}^{(1)}$, despite the fact that an extremely weak field at the one-photon level is input. This fact demonstrates the strong nonlinearity inherent in this system, which may appear even between individual photons.

4. Nonlinear Interaction Between Two Photons

In Sec. 3, the optical response of a cavity-QED system to classical light fields is analyzed. It was revealed that a cavity-QED system may exhibit significant nonlinear effects even by an extremely weak input field at the single photon level. Recent progress in photon generation techniques[19–24] has enabled the use of not only classical light fields but also individual photons (single photons, entangled photon pairs, etc.) as input for cavity QED-systems. In this section, we investigate theoretically the linear and nonlinear dynamics when two photons are simultaneously inputted into a cavity-QED system.

In the field of quantum optics, the interaction between photons mediated by nonlinear optical media has been briskly discussed.[29–31] However, the theories were

often based on a phenomenological interaction Hamiltonian with the single-mode approximation for photons, which is validated only when the input photons are off-resonant with the media and the media can be regarded as approximately dispersionless. Here, in order to maximize the nonlinear effect, we are also interested in the resonant region, where the system becomes highly dispersive and significant changes in the pulse shape are inevitable. Therefore, it is indispensable to use the Hamiltonian given by Eqs. (1)−(4), where the photon field is rigorously treated as a continuum.[32–36]

4.1. *Input and output wavefunctions*

Our main concern here is to investigate how the input one- and two-photon pulses are transformed after interaction with the atom-cavity system. The state vectors for the input one- and two-photon states are given by

$$|\Psi_{\rm in}^{(1)}\rangle = \int dr\psi(r)\tilde{b}_r^\dagger|0\rangle\,, \tag{61}$$

$$|\Psi_{\rm in}^{(2)}\rangle = 2^{-1/2}\int dr_1 dr_2\psi(r_1)\psi(r_2)\tilde{b}_{r_1}^\dagger\tilde{b}_{r_2}^\dagger|0\rangle\,, \tag{62}$$

where $\psi(r)$ denotes the input pulse shape, which is localized in the input port ($r<0$ region) and is normalized as $\int dr|\psi(r)|^2=1$. Throughout the present study, we discuss a case in which the two input photons have identical wavefunction $\psi(r)$, as given by Eq. (62).

After photons have interacted with the system, they appear either in the output field ($\tilde{b}_r^\dagger$ with $r>0$) or in the noncavity modes ($\tilde{d}_r^\dagger$). The output state vectors are denoted by[e]

$$|\Psi_{\rm out}^{(1)}\rangle = e^{-i\mathcal{H}t}|\Psi_{\rm in}^{(1)}\rangle = \int dr\bar{\psi}(r)\tilde{b}_r^\dagger|0\rangle + \cdots, \tag{63}$$

$$|\Psi_{\rm out}^{(2)}\rangle = e^{-i\mathcal{H}t}|\Psi_{\rm in}^{(2)}\rangle = 2^{-1/2}\int dr_1 dr_2\bar{\varphi}(r_1,r_2)\tilde{b}_{r_1}^\dagger\tilde{b}_{r_2}^\dagger|0\rangle + \cdots, \tag{64}$$

where the ellipses imply the terms containing photons in noncavity modes. The output two-photon wavefunction $\bar{\varphi}(r_1,r_2)$ has the symmetry of $\bar{\varphi}(r_2,r_1)=\bar{\varphi}(r_1,r_2)$ and is not factorizable in general, in contrast to the factorizable input wavefunction given by Eq. (62). Namely, two photons become correlated after the interaction mediated by nonlinear optical media. Except for the lossless case of $\gamma=0$, the output wavefunctions are attenuated, i.e. $\int dr|\bar{\psi}(r)|^2<1$ and $\int dr_1dr_2|\bar{\varphi}(r_1,r_2)|^2<1$.

[e]Strictly speaking, the output wavefunctions are dependent on the time t and should be denoted as, for example, $\bar{\psi}(r,t)$. However, if t is sufficiently larger than the interaction time, the output photons move at the speed of light while maintaining the pulse shape. The time variable t is thus omitted.

4.2. *Quantification of two-photon nonlinearity*

4.2.1. *Linear output two-photon wavefunction*

In order to quantify the nonlinear effect appearing in the output two-photon wavefunction $\bar{\varphi}(r_1, r_2)$, we define the *linear* output two-photon wavefunction $\bar{\varphi}_{\rm lin}(r_1, r_2)$. It is defined as the output from a linear system, i.e. a system in which the atoms are replaced with harmonic oscillators with the same transition frequencies, and therefore the atomic nonlinearity (saturation) is completely removed. In such linear systems, the two-photon output is simply obtained as a product of the one-photon output. Thus, $\bar{\varphi}_{\rm lin}(r_1, r_2)$ is given by

$$\bar{\varphi}_{\rm lin}(r_1, r_2) = \bar{\psi}(r_1)\bar{\psi}(r_2)\,. \tag{65}$$

4.2.2. *Measure of two-photon nonlinearity*

As the measure of two-photon nonlinearity, we employ the following complex number α:

$$\alpha = \frac{\displaystyle\int dr_1 dr_2 \bar{\varphi}^*_{\rm lin}(r_1, r_2)\bar{\varphi}(r_1, r_2)}{\displaystyle\sqrt{\int dr_1 dr_2 |\bar{\varphi}_{\rm lin}(r_1, r_2)|^2}\sqrt{\int dr_1 dr_2 |\bar{\varphi}(r_1, r_2)|^2}}\,, \tag{66}$$

which gives the *angle* between $\bar{\varphi}$ and $\bar{\varphi}_{\rm lin}$. α always lies in the unit circle ($|\alpha| \leq 1$) due to Schwartz's inequality, and $\alpha = 1$ when the response of the system is completely linear ($\bar{\varphi} = \bar{\varphi}_{\rm lin}$). Thus, the nonlinear effect appears as the deviation of α from unity. In the lossless case, the norms of $\bar{\varphi}$ and $\bar{\varphi}_{\rm lin}$ become unity, and α is simply reduced to the overlap integral between $\bar{\varphi}$ and $\bar{\varphi}_{\rm lin}$.

4.2.3. *Connection to controlled phase gates*

The strong optical nonlinearity that is sensitive to individual photons seems quite suitable for use in the construction of an optical quantum gate. Let us consider the optical circuit illustrated in Fig. 10, called the Fredkin gate.[18,30,47,48] The Fredkin gate is constructed by two 50:50 beamsplitters and two identical nonlinear optical system. As the nonlinear optical system, we consider here a lossless cavity QED system.

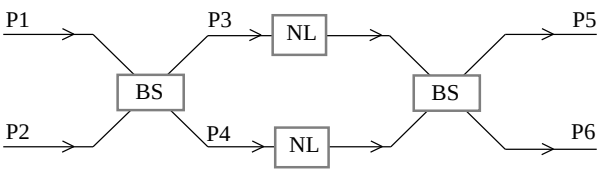

Fig. 10. Schematic diagram of the Fredkin gate, which is made up of two beamsplitters (BS) and two nonlinear optical systems (NL).

The circuit supports two input paths, P1 and P2. With respect to quantum gates, the following four input states are relevant:

$$|00\rangle = |0\rangle\,,$$
$$|10\rangle = B_1^\dagger|0\rangle\,,$$
$$|01\rangle = B_2^\dagger|0\rangle\,,$$
$$|11\rangle = B_1^\dagger B_2^\dagger|0\rangle\,,$$

where $B_j^\dagger \equiv \int dr\psi(r)b_{j,r}^\dagger$ creates a single photon with wavefunction $\psi(r)$ in Pj. Thus, the state $|m,n\rangle$ has m (n) photons in P1 (P2). The optical paths P1 and P2 are connected to P3 and P4 through the first beamsplitter. These paths are related by the following unitary transformation:

$$b_{1,r}^\dagger \to 2^{-1/2}(b_{3,r}^\dagger + b_{4,r}^\dagger)\,, \tag{67}$$

$$b_{2,r}^\dagger \to 2^{-1/2}(b_{3,r}^\dagger - b_{4,r}^\dagger)\,. \tag{68}$$

A remarkable role of a beamsplitter is that it transforms the $|11\rangle$ state as $B_1^\dagger B_2^\dagger|0\rangle \to 2^{-1}(B_3^\dagger B_3^\dagger - B_4^\dagger B_4^\dagger)|0\rangle$. Namely, two photons always appear in the same path (HOM interference[49]). The nonlinear systems placed in P3 and P4 make the following transformations on the one- and two-photon wavefunctions:

$$\psi(r) \to \bar{\psi}(r)\,, \tag{69}$$

$$\psi(r_1)\psi(r_2) \to \bar{\varphi}(r_1,r_2)\,. \tag{70}$$

The action of the second beamsplitter is the same as that of the first. Finally, the state vectors of the output photons appearing in P5 and P6 are given by

$$|00\rangle \to |0\rangle \equiv |\bar{0}\bar{0}\rangle\,, \tag{71}$$

$$|10\rangle \to \bar{B}_5^\dagger|0\rangle \equiv |\bar{1}\bar{0}\rangle\,, \tag{72}$$

$$|01\rangle \to \bar{B}_6^\dagger|0\rangle \equiv |\bar{0}\bar{1}\rangle\,, \tag{73}$$

$$|11\rangle \to \int dr_1 dr_2 \bar{\varphi}(r_1,r_2) b_{5,r_1}^\dagger b_{6,r_2}^\dagger|0\rangle\,, \tag{74}$$

where $\bar{B}_j^\dagger \equiv \int dr\bar{\psi}(r)b_{j,r}^\dagger$ creates a photon with $\bar{\psi}(r)$, and $|\bar{m},\bar{n}\rangle$ denotes a state with $\bar{m}$ ($\bar{n}$) photons with wavefunction $\bar{\psi}(r)$ in P5 (P6).

Now let us consider the connection to the measure α of two-photon nonlinearity. When $|\alpha| = 1$, the two-photon output wavefunction $\bar{\varphi}$ is necessarily given by

$$\bar{\varphi}(r_1,r_2) = \alpha\bar{\varphi}_{\rm lin}(r_1,r_2) = \alpha\bar{\psi}(r_1)\bar{\psi}(r_2)\,. \tag{75}$$

In this case, Eq. (74) is recast into the following form:

$$|11\rangle \to \alpha\bar{B}_5^\dagger\bar{B}_6^\dagger|0\rangle \equiv e^{i\theta}|\bar{1}\bar{1}\rangle\,, \tag{76}$$

where θ is the argument of α. By combining Eqs. (71), (72), (73) and (76), the action of this optical circuit is given by $|m,n\rangle \to \exp(imn\theta)|\bar{m},\bar{n}\rangle$. Thus, this gate

operates as a controlled phase gate, and α gives the phase factor of this gate. However, in general, the shape of $\bar{\varphi}$ is different from that of $\bar{\varphi}_{\rm lin}$ and $|\alpha|$ becomes smaller than unity. When $|\alpha|$ is considerably smaller than unity, this gate can no longer be regarded as a controlled phase gate.

4.3. *Connection to semiclassical theories*

In order to pursue the two-photon dynamics theoretically, the quantum-mechanical temporal evolution must be investigated while treating the two photonic continua (the input/output field and noncavity modes) as quantized fields. This analysis is carried out in Sec. 4.4 and Appendix C. Such a fully quantum-mechanical analysis is usually a heavy theoretical task, particularly when the optical media have many mechanical degrees of freedom. In contrast, if the input field is classical, as in Sec. 3, much simpler analysis is possible in the semiclassical framework, in which two photonic continua can be treated as classical (c-number) fields. Here, we show that the results of such a semiclassical analysis can be applied to evaluate the two-photon nonlinearity α, bypassing the fully quantum-mechanical analysis.[35]

For the purpose of considering the dynamics of two photons, the state vector of which is given by Eq. (62), we consider as the input state a classical pulse with mean amplitude $\psi(r)$. Since $\psi(r)$ is normalized as $\int dr|\psi(r)|^2 = 1$, this classical pulse contains one photon on average. The state vector of this classical pulse is given by

$$|\Psi_{\rm in}^{(\rm c)}\rangle = \exp\left(-\int dr|\psi(r)|^2/2\right)\exp\left(\int dr\psi(r)\tilde{b}_r^\dagger\right)|0\rangle\,, \tag{77}$$

which is composed of superposition of different number states, as is characteristic to the classical (coherent) state. Following the notations of Sec. 4.1 and assuming that the system is free from dissipation ($\gamma = 0$), the zero-, one-, and two-photon components are transformed, after the interaction with the system, as

$$|0\rangle \to |0\rangle\,, \tag{78}$$

$$\int dr\psi(r)\tilde{b}_r^\dagger|0\rangle \to \int dr\bar{\psi}(r)\tilde{b}_r^\dagger|0\rangle\,, \tag{79}$$

$$2^{-1/2}\int dr_1dr_2\psi(r_1)\psi(r_2)\tilde{b}_{r_1}^\dagger\tilde{b}_{r_2}^\dagger|0\rangle \to 2^{-1/2}\int dr_1dr_2\bar{\varphi}(r_1,r_2)\tilde{b}_{r_1}^\dagger\tilde{b}_{r_2}^\dagger|0\rangle\,. \tag{80}$$

Thus, for up to two-photon states, the output wavefunction is given by

$$|\Psi_{\rm out}\rangle = \exp\left(-\int dr\frac{|\psi(r)|^2}{2}\right)\left[1+\int dr\bar{\psi}(r)\tilde{b}_r^\dagger + \int dr_1dr_2\frac{\bar{\varphi}(r_1,r_2)}{2}\tilde{b}_{r_1}^\dagger\tilde{b}_{r_2}^\dagger\right]|0\rangle\,. \tag{81}$$

Using this output wavefunction, the output field amplitude $f_{\rm out}(r) = \langle\Phi_{\rm out}|\tilde{b}_r|\Phi_{\rm out}\rangle$

is given, up to the third-order response, by

$$f_{\rm out}(r) = f^{(1)}_{\rm out}(r) + f^{(3)}_{\rm out}(r) + \mathcal{O}(f^{(5)}_{\rm out})\,, \tag{82}$$

$$f^{(1)}_{\rm out}(r) = \bar{\psi}(r)\,, \tag{83}$$

$$f^{(3)}_{\rm out}(r) = \int dr' \bar{\psi}^*(r')\bar{\varphi}(r,r') - \bar{\psi}(r)\int dr' |\bar{\psi}(r')|^2\,. \tag{84}$$

The linear output $f^{(1)}_{\rm out}(r)$ is identical to the one-photon output wavefunction $\bar{\psi}(r)$, while the third-order output $f^{(3)}_{\rm out}(r)$ contains contracted information of the two-photon output wavefunction $\bar{\varphi}(r_1, r_2)$. Remembering that $\bar{\psi}(r)$ is normalized as $\int dr|\bar{\psi}(r)|^2 = 1$, it is confirmed that the following quantity,

$$\alpha' = 1 + \int dr (f^{(1)}_{\rm out}(r))^* f^{(3)}_{\rm out}(r)\,, \tag{85}$$

is identical to the two-photon nonlinearity parameter α defined by Eq. (66). As will be confirmed numerically in Sec. 4.4, α and α' show complete agreement. Thus, we can evaluate the two-photon nonlinearity parameter α from $f^{(1)}_{\rm out}(r)$ and $f^{(3)}_{\rm out}(r)$, which are the linear and the third-order output fields for a *classical* input field with mean amplitude $\psi(r)$. Since these quantities can be calculated within the semiclassical theory, as in Sec. 3.3, one can determine α while avoiding fully quantum-mechanical calculation.

In the above discussion, it is assumed that the input photons appear in the output port without leaving any elementary excitations in the system. However, no system-dependent features are used. Therefore, this semiclassical evaluation method is applicable to any optical system in the dissipation-free limit. This method would be particularly valuable in evaluating the two-photon nonlinearity in complex systems, such as excitonic systems (see Sec. 4.5), where full quantum-mechanical analyses are much more difficult than semiclassical analyses.

4.4. *Single-atom in a cavity*

Here, we actually evaluate the measure α of two-photon nonlinearity for the simplest case of a single atom in a cavity. To this end, two distinct analyses are used. One is a fully quantum-mechanical analysis, where temporal evolution of the input photons is pursued by solving the Schrödinger equation. The one- and two-photon propagators, denoted by $G_{r'\to r}(t)$ and $G_{r'_1,r'_2\to r_1,r_2}(t)$, respectively, are obtained analytically, as shown in Appendix C. The one- and two-photon output wavefunctions are given by

$$\bar{\psi}(r) = \int dr' G_{r'\to r}(t)\psi(r')\,, \tag{86}$$

$$\bar{\varphi}(r_1, r_2) = \int dr'_1 dr'_2 G_{r'_1,r'_2\to r_1,r_2}(t)\psi(r'_1)\psi(r'_2)\,. \tag{87}$$

The target quantity α is evaluated by Eq. (66). In this method, complete information on the output photons (photonic correlations, etc.) can be accessed in terms of the two-photon wavefunction, $\bar{\varphi}$.

The other method is a semiclassical analysis discussed in Sec. 4.3. This is much simpler theoretical analysis compared to the fully quantum-mechanical analysis. However, only a limited class of information on the output photons is available, since a contracted wavefunction [the first term in the right hand side of Eq. (84)] is calculated effectively.

In Secs. 4.4 and 4.5, a Gaussian wavepacket is employed for input photons:

$$\psi(r) = \left(\frac{2}{\pi d^2}\right)^{1/4} \exp\left(-\frac{r^2}{d^2} + i(\omega_c + q)r\right). \tag{88}$$

The parameters that characterize this wavefunction are the central frequency q (measured from the cavity frequency) and the coherent length d.

4.4.1. *Numerical results*

Here, we present the numerical results obtained for the lossless cases of $\gamma = 0$. The atom-cavity system is then characterized solely by the ratio κ/g. Recalling Sec. 2.2.1, the weak (strong) coupling regime is specified by the inequality $\kappa/g \gtrsim 4$ ($\kappa/g \lesssim 4$).

The numerical results for weak coupling cases ($\kappa/g = 5, 10$) are plotted in Fig. 11, where the magnitude of nonlinearity is evaluated by $|\alpha - 1|$. The frequency of input photons is set at $q = 0$, since the resonance condition is given by $q = 0$ in the weak coupling regime and nonlinearity appears most strongly at this frequency. Figure 11 indicates that $|\alpha - 1|$ depends solely on $g^2 d/\kappa$ in the weak coupling regime. As discussed in Sec. 2.3.3, the atom-cavity system in this regime may be regarded

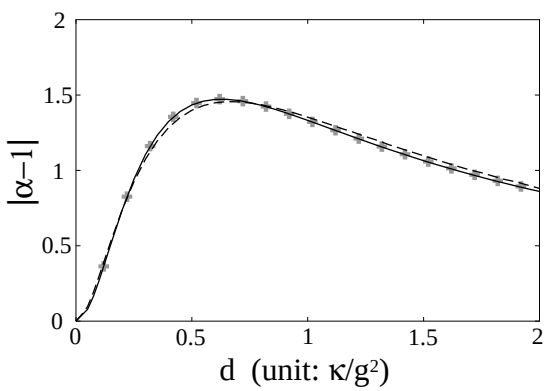

Fig. 11. Dependence of $|\alpha - 1|$ on the pulse length d. The solid and dashed lines show the results for $\kappa/g = 5$ and $\kappa/g = 10$, respectively. The gray cross marks indicate the results for $\kappa/g = 5$ calculated by the semiclassical evaluation method. The frequency of the photons is $q = 0$.

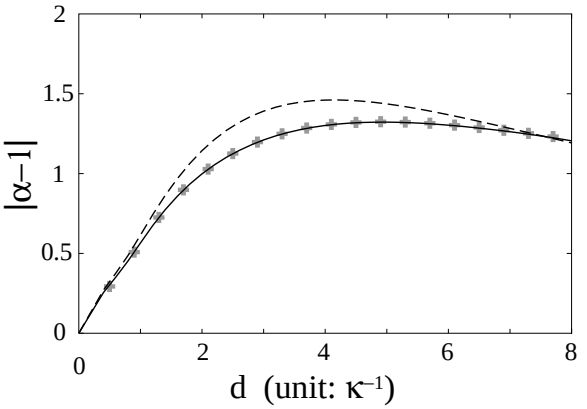

Fig. 12. Dependence of $|\alpha - 1|$ on the pulse length d in the strong coupling regime, $\kappa/g = 0.5$. The input frequency is set at $q/g = 0.9$ (dashed line) and $q/g = 1$ (solid line). The gray cross marks indicate the results for $q/g = 1$ calculated by the semiclassical evaluation method.

as a "one-dimensional atom" with a coupling constant of $\Gamma = 4g^2/\kappa$. The optimum pulse length to maximize the nonlinearity is given by $d \sim 0.5\kappa/g^2$.

The numerical results for a strong coupling case ($\kappa/g = 0.5$) are plotted in Fig. 12. In contrast to the weak coupling regime, weak nonlinearity results for the $q = 0$ photons, since they are no longer resonant due to the Rabi splitting of the eigenenergies of the atom-cavity system. Instead, large nonlinearity is obtained when the input photons are tuned to the Rabi-split frequency, $q \sim \pm g$. The maximum value of $|\alpha - 1|$ is approximately 1.5, which is approximately the same as the value reached in the weak coupling regime. The optimum pulse length is given by $d \sim 4/\kappa$.

In Figs. 11 and 12, the lines represent the results obtained by the fully quantum-mechanical formalism, and the gray cross marks represent the results obtained by the semiclassical formalism. The validity of the semiclassical evaluation method is proved by their complete agreement.

4.4.2. *Optimum pulse for maximizing nonlinearity*

In Sec. 4.4.1, the optimum frequency q and the length d for maximizing the nonlinearity are clarified to be $(d, q) \sim (0.5\kappa/g^2, 0)$ in the weak coupling regime and $(d, q) \sim (4/\kappa, \pm g)$ in the strong coupling regime. Here, we account for these optimum conditions from a unified perspective.

To this end, we consider such a single photon pulse $\psi_{\rm opt}(r)$ that will completely be absorbed by the atom. This single photon pulse is determined by

$$e^{i\mathcal{H}t}s^\dagger|0\rangle = \int dr \psi_{\rm opt}(r) b_r^\dagger |0\rangle \,, \tag{89}$$

where t is much larger than the atomic radiative lifetime. If the input pulse $\psi(r)$

resembles $\psi_{\rm opt}(r)$ in shape, the two input photons try to occupy the atom simultaneously and strong nonlinear effects are expected.

$\psi_{\rm opt}(r)$ has the following form:

$$\psi_{\rm opt}(r) = \begin{cases} \dfrac{ig\kappa^{1/2}}{\tilde{\omega}_1^* - \tilde{\omega}_2^*} \left(e^{i\tilde{\omega}_1^*(r+t)} - e^{i\tilde{\omega}_2^*(r+t)}\right) & (-t < r < 0) \\ 0 & (\text{otherwise})\,, \end{cases} \tag{90}$$

where $\tilde{\omega}_1$ and $\tilde{\omega}_2$ are the complex eigenfrequencies defined in Eq. (14). In the weak coupling regime, $\tilde{\omega}_1$ and $\tilde{\omega}_2$ are approximately given by $-i\kappa/2$ and $-2ig^2/\kappa$. Because $\kappa \gg g^2/\kappa$ in this regime, the optimum frequency q and pulse length d are given by $q \sim 0$ and $d \sim \kappa/2g^2$. On the other hand, in the strong coupling regime, $\tilde{\omega}_1$ and $\tilde{\omega}_2$ are approximately given by $-i\kappa/4 \pm g$. Therefore, the optimum q and d are roughly estimated at $q \sim \pm g$ and $d \sim 4/\kappa$.

4.5. *Excitonic system in a cavity*

In Sec. 4.4, we have evaluated the two-photon nonlinearity obtained by a single two-level atom inside of a cavity. However, optical media have many more mechanical degrees of freedom in general and cannot be modeled by a single two-level system. Here, as an example of more complicated optical systems, we discuss a Frenkel excitonic system placed in a cavity.[36] (This model is also applicable to atomic gas systems by neglecting the hopping interaction between the sites.)

4.5.1. *Model and method*

A Frenkel excitonic system is modeled by N identical two-level systems (called "atoms") with the excitation-hopping interaction among them. Generalizing Eq. (2), the system part of the Hamiltonian is given by

$$\mathcal{H}'_{\rm sys} = \omega_{\rm a} \sum_j s_j^\dagger s_j + \omega_{\rm c} c^\dagger c + g \sum_j (s_j^\dagger c + c^\dagger s_j) + \sum_{j \neq i} V_{ji} s_j^\dagger s_i\,, \tag{91}$$

where $j (= 1, \ldots, N)$ is the site index and the last term describes the hopping interaction. In general, the atom-cavity coupling g depends on j through the locations of each site and the directions of the transition dipole moments; however, this j dependence is negligible in Frenkel excitonic systems since the atoms are closely arranged. As the form of V_{ji}, we employ the following mean-field form:[f]

$$V_{ji} = \begin{cases} -\dfrac{V}{N-1} & (j \neq i) \\ 0 & (j = i)\,. \end{cases} \tag{92}$$

[f]The results are qualitatively unchanged if we choose a more realistic form of V_{ji}, such as the nearest-neighbor coupling.[36]

The ground state is given by $|\mathrm{x}_1\rangle = \sum_{j=1}^{N} N^{-1/2} s_j^\dagger |0\rangle$, the eigenenergy of which is given by $\omega_\mathrm{a} - V$. Other levels lie at $\omega_\mathrm{a} + V/(N-1)$ with $(N-1)$-fold degeneracy. We hereinafter treat the case in which the ground state is resonant with the cavity, i.e. $\omega_\mathrm{a} - V = \omega_\mathrm{c}$, and set $\omega_\mathrm{a} - V(= \omega_\mathrm{c})$ as the origin of the frequency. The coupling strength between the cavity mode and the ground state is given by $\sqrt{N}g$, whereas other eigenstates completely lose coupling to the cavity mode.

If the hopping interaction is not present, all of the atomic levels are degenerate. Therefore, the nonlinearity inherent in the system due to saturation effect is expected to be weakened as the system size N increases. However, the hopping interaction lifts the degeneracy and would recover the saturation effect. In particular, if the energy separation V exceeds by far the other relevant energy scales, the system would behave as an *effective* two-level system, showing strong nonlinearity. These points will be revealed in the following calculations.

The calculation of the two-photon nonlinearity is carried out by the semiclassical method discussed in Sec. 4.3. Assuming the lossless limit of $\gamma \to 0$, the Hamiltonian of the whole system is given by $\mathcal{H}' = \mathcal{H}'_\mathrm{sys} + \mathcal{H}_\mathrm{ce}$, where $\mathcal{H}'_\mathrm{sys}$ and $\mathcal{H}_\mathrm{ce}$ are given by Eqs. (91) and (3), respectively. The resulting semiclassical equations are presented in Appendix B.

4.5.2. *Results*

In order to observe the size effects, the two-photon nonlinearity parameter α is plotted on the complex plane in Fig. 13, varying the system size N. The system is in the strong coupling regime ($\kappa/g = 0.5$). The hopping interaction exists in Fig. 13(a) and does not exist in Fig. 13(b). Regarding input photons, the optimum pulse shape revealed in Sec. 4.4.2 is assumed. Since the atom-cavity coupling is size-enhanced to be $\sqrt{N}g$, the optimum pulse is given by $d = 4/\kappa$ and $q = -\sqrt{N}g$ (the lower Rabi-split frequency).

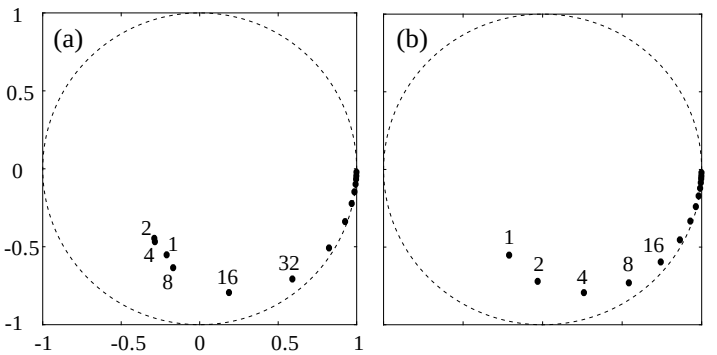

Fig. 13. Plot of α on the complex plane. The dotted line shows the unit circle. The integers near each point represent the system size N. For each N, the optimum pulse shape for maximizing nonlinearity is employed. The system parameters are chosen as follows: $\kappa/g = 0.5$, $\omega_\mathrm{a} - V = \omega_\mathrm{c}$, and $V/g = 5$ in (a) and 0 in (b).

In Fig. 13(b), in which all of the atomic levels are degenerate, the two-photon nonlinearity due to saturation effect becomes weaker monotonously as N increases. In Fig. 13(a), in which the degeneracy is lifted by the finite hopping interaction, α remains almost unchanged if the system size is small ($N \lesssim 10$). This is because the lowest excitonic state behaves as an isolated level due to the large energy separation. Thus, a quantum dot can be regarded as an "artificial two-level atom" although they are actually composed of many two-level atoms.

It is commonly observed in both figures that the two-photon nonlinearity becomes weaker as the system size N becomes larger ($\alpha \to 1$ as $N \to \infty$), as expected. For large N, the nonlinear effect mainly appears in the phase of α, keeping $|\alpha| \simeq 1$. In other words, for large N, the nonlinear effect appears as the nonlinear phase shift in the output wavefunction, keeping the shape of the output pulse unchanged from the linear case.

5. Summary

It has been pointed out that induction of nonlinear optical effects by only two photons would be possible by utilizing the field-amplification effect of a cavity. In the present article, we have reviewed our recent analysis on the two-photon dynamics occurring in a cavity-QED system. Since a cavity-QED system is highly dispersive around its resonances, phenomenological treatments based on the single-mode approximation cannot be applied. Our analysis is based on a theoretical model in which the external photon field is treated rigorously as a continuum, which enables us to handle the photonic wavefunction in the spatial representation.

In Sec. 2, the Hamiltonian describing a cavity-QED system is presented, and its basic properties are discussed. The Hamiltonian includes three principal parameters: the atom-cavity coupling g, the damping rate κ of the cavity mode, and the radiative decay rate γ of the atom into non-cavity modes. In a cavity-QED system, the atom placed inside of a cavity is coupled to two kinds of photonic continua, namely, the quasi-cavity continuum and non-cavity modes. We have observed how the three parameters are reflected in the form factors for the atom-photon interaction. The method by which to determine the cavity-QED parameters for a planar cavity is also discussed.

In Sec. 3, the optical response of a cavity-QED system to classical light fields (coherent state) is investigated. In this case, the input fields can be treated as c-number fields. In other words, a semiclassical theory is rigorously derived from a fully quantum-mechanical formalism. In Sec. 3.3, we examined the optical response to an extremely weak input pulse at the single-photon level. If the input pulse is resonant with the cavity-QED system, the shape of the output pulse is deformed significantly from the input as shown in Fig. 9(b), suggesting inapplicability of the single-mode approximation. Furthermore, the third-order response has a comparable magnitude to that of the linear response, indicating a strong optical nonlinear effect, even by a weak input field at the single-photon level.

In Sec. 4, the dynamics of two photons inputted simultaneously into a cavity-QED system is investigated. The wavefunction of the output photons is calculated using the propagator presented in Appendix C, and the optical nonlinearity appearing in the output wavefunction is quantified by comparing it with the linear output wavefunction. The results of the semiclassical theory presented in Sec. 3.3 can be applied for evaluation of this two-photon nonlinearity. When the cavity contains only one atom, significant two-photon nonlinearity can be induced by choosing optimal pulse shapes for the input photons. As the number of atoms increases, the nonlinear effect becomes smaller. However, if the hopping interaction exists between atoms (e.g. Frenkel exciton system), it lifts the degeneracy of atomic energies and revives the two-photon nonlinearity. As is shown in Fig. 13, the two-photon nonlinearity appears not purely as a phase shift in the output wavefunction. The degradation of the fidelity between the output wavefunction and the linear output wavefunction always occurs, which hinders application of this nonlinear effect as a quantum phase gate. However, the large two-photon optical nonlinearity attainable in cavity-QED systems will likely find other novel applications in future quantum control technology.

Acknowledgments

The authors are grateful to Y. Shinozuka, H. Ajiki, M. Bamba, K. Edamatsu, G. Oohata and K. Miyajima for fruitful discussions. This research was partially supported by the following three grants: (i) CREST project of Japan Science and Technology Agency, (ii) the Research Foundation for Opto-Science and Technology, and (iii) Grant-in-Aid for Creative Scientific Research (17GS1204).

Appendix A. Form Factors for a Planar Cavity Geometry

Here, we derive the form factors of Eqs. (29) and (30) from the three-dimensional Hamiltonian of Eq. (27). First, we diagonalize the photonic part of the Hamiltonian. Recall here that the in-plane wavevector $\vec{k}$ is conserved in the interaction between $c_{\vec{k}}$ and $b_{\boldsymbol{k}}$. The eigenmode operator $B_{\vec{k}\omega}$ (with the in-plane wavevector $\vec{k}$ and the eigenfrequency ω) is given, after employing an approximation of $\omega_{\boldsymbol{k}} \simeq k_z$, by

$$B_{\vec{k}\omega} = \eta_{\vec{k}}(\omega) c_{\vec{k}} + \int dk_z \zeta_{\vec{k}}(\omega, k_z) b_{\boldsymbol{k}} \,, \tag{A.1}$$

where

$$\eta_{\vec{k}}(\omega) = \frac{(2\pi\tau_{\vec{k}})^{-1/2}}{\omega - \omega_{\vec{k}} + i/2\tau_{\vec{k}}} \,, \tag{A.2}$$

$$\zeta_{\vec{k}}(\omega, k_z) = \frac{(2\pi\tau_{\vec{k}})^{-1}}{(\omega - \omega_{\vec{k}} + i/2\tau_{\vec{k}})(\omega - k_z + i\delta)} + \delta(\omega - k_z) \,. \tag{A.3}$$

$B_{\vec{k}\omega}$ is normalized as $[B_{\vec{k}\omega}, B^\dagger_{\vec{k}'\omega'}] = \delta^2(\vec{k}-\vec{k}')\delta(\omega-\omega')$. Inversely, $c_{\vec{k}} = \int d\omega \eta^*_{\vec{k}}(\omega) B_{\vec{k}\omega}$. In terms of $B_{\vec{k}\omega}$, the original Hamiltonian of Eq. (27) is recast into the following form:

$$\mathcal{H}_{\rm planar} = \omega_{\rm a} s^\dagger s + \int d^2\vec{k} d\omega [(\lambda_{\vec{k}} \eta^*_{\vec{k}}(\omega) s^\dagger B_{\vec{k}\omega} + {\rm H.c.}) + \omega B^\dagger_{\vec{k}\omega} B_{\vec{k}\omega}] \,. \tag{A.4}$$

From this form of Hamiltonian, the overall form factor is readily obtained as

$$|\xi_{\rm t}(\omega)|^2 = \int d^2\vec{k} |\lambda_{\vec{k}} \eta_{\vec{k}}(\omega)|^2 \,. \tag{A.5}$$

Next, we determine the quasi-cavity continuum. The input photon profile now becomes important at this stage. Choosing a single-photon state as input, its state vector is given by

$$|in\rangle = \int d^3\boldsymbol{r} \varphi(x,y)\psi(z) b^\dagger_{\boldsymbol{r}} |0\rangle \,, \tag{A.6}$$

where $\psi(z)$ is the vertical profile of the input photon, which is localized in the $z<0$ region and is normalized as $\int dz |\psi(z)|^2 = 1$, and $b_{\boldsymbol{r}}$ is the annihilation operator for the external field in the space representation, $b_{\boldsymbol{r}} = (2\pi)^{-3/2} \int d^3\boldsymbol{k} e^{i\boldsymbol{k}\cdot\boldsymbol{r}} b_{\boldsymbol{k}}$. Denoting the Fourier transforms of $\varphi(x,y)$ and $\psi(z)$ by $\tilde{\varphi}(\vec{k})$ and $\tilde{\psi}(k_z)$, respectively, the above state vector can be rewritten as

$$|in\rangle = \int d^2\vec{k} d\omega \tilde{\psi}(\omega) \tilde{\varphi}(\vec{k}) \frac{\eta_{\vec{k}}(\omega)}{\eta^*_{\vec{k}}(\omega)} B^\dagger_{\vec{k}\omega} |0\rangle \,. \tag{A.7}$$

To relate the present problem to the conventional (g,κ,γ)-model, the quasi-cavity continuum should be defined so as to contain the input photon state completely. The quasi-cavity continuum C_ω is thus defined by

$$C^\dagger_\omega = \int d^2\vec{k} \tilde{\varphi}(\vec{k}) \frac{\eta_{\vec{k}}(\omega)}{\eta^*_{\vec{k}}(\omega)} B^\dagger_{\vec{k}\omega} \,. \tag{A.8}$$

Note that C_ω is normalized as $[C_\omega, C^\dagger_{\omega'}] = \delta(\omega-\omega')$. Thus, $|\xi_{\rm c}(\omega)|^2$ is given by

$$|\xi_{\rm c}(\omega)|^2 = |\langle 0| s \mathcal{H}_{\rm planar} C^\dagger_\omega |0\rangle|^2 = \left| \int d^2\vec{k} \tilde{\varphi}(\vec{k}) \lambda_{\vec{k}} \eta_{\vec{k}}(\omega) \right|^2 \,. \tag{A.9}$$

Appendix B. Semiclassical Equations for Excitonic Systems

Here, we present the semiclassical equations of motion for an excitonic system in a cavity, up to the third-order quantities. The Hamiltonian upon which these equations are based is given by Eq. (91). The equations for the single atom case, which have been used in the analysis of Sec. 3.3, can be obtained by setting $V_{ji} = 0$. (Note that $\langle s_m s_n \rangle$, $\langle s^\dagger_m s_n s_l \rangle$ and $\langle c^\dagger s_m s_n \rangle$ vanish because $ss = 0$ in the single atom case.)

Dividing $\langle c\rangle$ and $\langle s_m\rangle$ into the linear and third-order components as $\langle c\rangle = \langle c_1\rangle + \langle c_3\rangle$ and $\langle s_m\rangle = \langle s_{1,m}\rangle + \langle s_{3,m}\rangle$, and denoting the detuning $\omega_{\rm a} - \omega_{\rm c}$ by Ω, the equations of motion for the linear quantities are given by

$$\frac{d}{dt}\langle c_1\rangle = -\frac{\kappa}{2}\langle c_1\rangle - ig\sum_j \langle s_{1,j}\rangle - i\sqrt{\kappa}f_{\rm in}(t_0 - t)\,, \tag{B.1}$$

$$\frac{d}{dt}\langle s_{1,m}\rangle = -i\Omega\langle s_{1,m}\rangle - i\sum_{j(\neq m)} V_{mj}\langle s_{1,j}\rangle - ig\langle c_1\rangle\,. \tag{B.2}$$

The equations of motion for the second-order quantities are given by

$$\frac{d}{dt}\langle s_m^\dagger s_n\rangle = i\sum_{j(\neq m)} V_{jm}\langle s_j^\dagger s_n\rangle - i\sum_{j(\neq n)} V_{nj}\langle s_m^\dagger s_j\rangle - ig(\langle s_m^\dagger c\rangle - \langle s_n^\dagger c\rangle^*)\,, \tag{B.3}$$

$$\begin{aligned}\frac{d}{dt}\langle s_m^\dagger c\rangle = {}& (i\Omega - \frac{\kappa}{2})\langle s_m^\dagger c\rangle + i\sum_{j(\neq m)} V_{jm}\langle s_j^\dagger c\rangle - ig\sum_j \langle s_m^\dagger s_j\rangle + ig\langle c^\dagger c\rangle \\ & -i\sqrt{\kappa}f_{\rm in}(t_0 - t)\langle s_{1,m}\rangle^*\,,\end{aligned} \tag{B.4}$$

$$\frac{d}{dt}\langle c^\dagger c\rangle = -\kappa\langle c^\dagger c\rangle + ig\sum_j(\langle s_j^\dagger c\rangle - \text{c.c.}) + (i\sqrt{\kappa}f^*(t_0 - t)\langle c_1\rangle + \text{c.c.})\,, \tag{B.5}$$

$$\begin{aligned}\frac{d}{dt}\langle s_m s_n\rangle = {}& -2i\Omega\langle s_m s_n\rangle - i\sum_{j(\neq m)} V_{mj}\langle s_j s_n\rangle - i\sum_{j(\neq n)} V_{nj}\langle s_m s_j\rangle \\ & - ig(\langle s_n c\rangle + \langle s_m c\rangle)\,,\end{aligned} \tag{B.6}$$

$$\begin{aligned}\frac{d}{dt}\langle s_m c\rangle = {}& \left(-i\Omega - \frac{\kappa}{2}\right)\langle s_m c\rangle - i\sum_{j(\neq m)} V_{mj}\langle s_j c\rangle - ig\langle cc\rangle \\ & - ig\sum_j \langle s_m s_j\rangle - i\sqrt{\kappa}f_{\rm in}(t_0 - t)\langle s_{1,m}\rangle\,,\end{aligned} \tag{B.7}$$

$$\frac{d}{dt}\langle cc\rangle = -\kappa\langle cc\rangle - 2ig\sum_j \langle s_j c\rangle - 2i\sqrt{\kappa}f_{\rm in}(t_0 - t)\langle c_1\rangle\,. \tag{B.8}$$

The equations of motion for the third-order quantities are given by

$$\begin{aligned}\frac{d}{dt}\langle s_m^\dagger s_n s_l\rangle = {}& -i\Omega\langle s_m^\dagger s_n s_l\rangle + i\sum_{j(\neq m)} V_{jm}\langle s_j^\dagger s_n s_l\rangle - i\sum_{j(\neq n)} V_{nj}\langle s_m^\dagger s_j s_l\rangle \\ & - i\sum_{j(\neq l)} V_{lj}\langle s_m^\dagger s_n s_j\rangle + ig(\langle c^\dagger s_n s_l\rangle - \langle s_m^\dagger s_l c\rangle - \langle s_m^\dagger s_n c\rangle)\,,\end{aligned} \tag{B.9}$$

$$\frac{d}{dt}\langle s_m^\dagger s_n c\rangle = -\frac{\kappa}{2}\langle s_m^\dagger s_n c\rangle + i\sum_{j(\neq m)} V_{jm}\langle s_j^\dagger s_n c\rangle - i\sum_{j(\neq n)} V_{nj}\langle s_m^\dagger s_j c\rangle + ig(\langle c^\dagger s_n c\rangle - \langle s_m^\dagger cc\rangle) - ig\sum_j \langle s_m^\dagger s_n s_j\rangle - i\sqrt{\kappa} f_{\rm in}(t_0-t)\langle s_m^\dagger s_n\rangle\,, \tag{B.10}$$

$$\frac{d}{dt}\langle s_m^\dagger cc\rangle = (i\Omega-\kappa)\langle s_m^\dagger cc\rangle + i\sum_{j(\neq m)} V_{jm}\langle s_j^\dagger cc\rangle - 2ig\sum_j \langle s_m^\dagger s_j c\rangle + ig\langle c^\dagger cc\rangle - 2i\sqrt{\kappa} f_{\rm in}(t_0-t)\langle s_m^\dagger c\rangle\,, \tag{B.11}$$

$$\frac{d}{dt}\langle c^\dagger s_m s_n\rangle = \left(-2i\Omega-\frac{\kappa}{2}\right)\langle c^\dagger s_m s_n\rangle - i\sum_{j(\neq m)} V_{mj}\langle c^\dagger s_j s_n\rangle - i\sum_{j(\neq n)} V_{nj}\langle c^\dagger s_m s_j\rangle - ig(\langle c^\dagger s_n c\rangle + \langle c^\dagger s_m c\rangle) + ig\sum_j \langle s_j^\dagger s_m s_n\rangle + i\sqrt{\kappa} f^*(t_0-t)\langle s_m s_n\rangle\,, \tag{B.12}$$

$$\frac{d}{dt}\langle c^\dagger s_m c\rangle = (-i\Omega-\kappa)\langle c^\dagger s_m c\rangle - i\sum_{j(\neq m)} V_{mj}\langle c^\dagger s_j c\rangle + ig\sum_j \langle s_j^\dagger s_m c\rangle - ig\sum_j \langle c^\dagger s_m s_j\rangle - ig\langle c^\dagger cc\rangle + i\sqrt{\kappa} f^*(t_0-t)\langle s_m c\rangle - i\sqrt{\kappa} f_{\rm in}(t_0-t)\langle c^\dagger s_m\rangle\,, \tag{B.13}$$

$$\frac{d}{dt}\langle c^\dagger cc\rangle = -\frac{3\kappa}{2}\langle c^\dagger cc\rangle + ig\sum_j \langle s_j^\dagger cc\rangle - 2ig\sum_j \langle c^\dagger s_j c\rangle + i\sqrt{\kappa} f^*(t_0-t)\langle cc\rangle - 2i\sqrt{\kappa} f_{\rm in}(t_0-t)\langle c^\dagger c\rangle\,, \tag{B.14}$$

$$\frac{d}{dt}\langle c_3\rangle = -\frac{\kappa}{2}\langle c_3\rangle - ig\sum_j \langle s_{3,j}\rangle\,, \tag{B.15}$$

$$\frac{d}{dt}\langle s_{3,m}\rangle = -i\Omega\langle s_{3,m}\rangle - i\sum_{j(\neq m)} V_{mj}\langle s_{3,j}\rangle - ig\langle c_3\rangle + 2ig\langle s_m^\dagger s_m c\rangle + 2i\sum_{j(\neq m)} V_{mj}\langle s_m^\dagger s_m s_j\rangle\,. \tag{B.16}$$

Appendix C. Propagators

In this Appendix, we outline the derivation of the one- and two-photon propagators for the single-atom case. Our starting point is the Hamiltonian of the form of Eq. (19). We use the following abbreviations for the atom-photon coupling constants,

$$g_k = g\eta^*(k) = \sqrt{\frac{g^2\kappa}{2\pi}}\,\frac{1}{k-\tilde{\omega}_{\rm c}^*}\,, \tag{C.1}$$

$$\gamma_k = \sqrt{\frac{\gamma}{2\pi}}\,. \tag{C.2}$$

C.1. *One-photon propagator*

The one-photon propagator is defined by

$$G_{r'\to r}(t) = \langle \tilde{b}_r e^{-i\mathcal{H}t}\tilde{b}_{r'}^\dagger\rangle_{\rm v}\,, \tag{C.3}$$

where $r' < 0 < r$, and $\langle\cdots\rangle_{\rm v}$ indicates a vacuum expectation value, i.e. $\langle\cdots\rangle_{\rm v} \equiv \langle 0|\cdots|0\rangle$. Using Eq. (18) and noting that $r' < 0 < r$, one can switch to the wavenumber space:

$$G_{r'\to r}(t) = \frac{i}{(2\pi)^2}\int dk dk' d\omega e^{i(kr-k'r'-\omega t)}\frac{\eta(k')}{\eta^*(k')}\left\langle C_k\frac{1}{\omega-\mathcal{H}+i\delta}C_{k'}^\dagger\right\rangle_{\rm v}\,, \tag{C.4}$$

C.1.1. *Green's function method*

Here, we evaluate the resolvent in Eq. (C.4), using the Green's function method. First, we define the *bare* Green functions for the atom and photons. These bare Green's functions are related to the free dynamics of the atom and photons. Denoting the non-interacting Hamiltonian by $\mathcal{H}_0$, they are given by

$$A(\omega) = \left\langle s\frac{1}{\omega-\mathcal{H}_0+i\delta}s^\dagger\right\rangle_{\rm v} = \frac{1}{\omega-\omega_{\rm a}+i\delta}\,, \tag{C.5}$$

$$\begin{aligned} P_{k'\to k}(\omega) &= \left\langle C_k\frac{1}{\omega-\mathcal{H}_0+i\delta}C_{k'}^\dagger\right\rangle_{\rm v} \\ &= \frac{\delta(k-k')}{\omega-k+i\delta} \equiv \delta(k-k')Q(\omega-k)\,. \end{aligned} \tag{C.6}$$

In the Feynman diagrams, these bare Green's functions are represented by solid and dotted lines, as shown in Figs. C.1(a) and C.1(b).

The *dressed* atomic Green's function, which includes the effects of the atom-photon interaction, is defined by

$$\bar{A}(\omega) = \left\langle s\frac{1}{\omega-\mathcal{H}+i\delta}s^\dagger\right\rangle_{\rm v}\,. \tag{C.7}$$

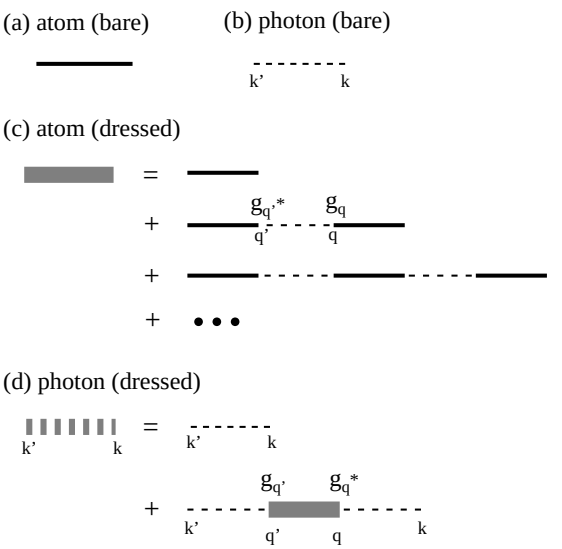

Fig. C.1. Feynman diagrams for the one-particle problem: (a) bare atomic Green's function, $A(\omega)$, (b) bare photonic Green's function, $P_{k'\to k}(\omega)$, (c) bare atomic Green's function, $\bar{A}(\omega)$, and (d) bare atomic Green's function, $\bar{P}_{k'\to k}(\omega)$.

It is known that the dressed atomic Green's function can be expanded in terms of the bare Green's functions as follows:

$$\begin{aligned}\bar{A}(\omega) &= A(\omega) + A(\omega)\Sigma(\omega)A(\omega) + A(\omega)\Sigma(\omega)A(\omega)\Sigma(\omega)A(\omega) + \cdots \\ &= \frac{A(\omega)}{1 - A(\omega)\Sigma(\omega)}\,, \end{aligned} \tag{C.8}$$

where $\Sigma(\omega)$, which is referred to as the self-energy, is given by

$$\Sigma(\omega) = \int dq' dq (g^*_{q'} g_q + \gamma^*_{q'}\gamma_q) P_{q'\to q}(\omega) = \frac{g^2}{\omega - \tilde{\omega}_{\rm c}} - \frac{i\gamma}{2}\,. \tag{C.9}$$

The Feynman diagrams corresponding to Eq. (C.8) are drawn in Fig. C.1(c). Combining Eqs. (C.8) and (C.9), the dressed atomic Green's function is given by

$$\bar{A}(\omega) = \frac{\omega - \tilde{\omega}_{\rm c}}{(\omega - \tilde{\omega}_1)(\omega - \tilde{\omega}_2)}\,, \tag{C.10}$$

where $\tilde{\omega}_1$ and $\tilde{\omega}_2$ are the complex eigenfrequencies of the atom-cavity system defined by Eq. (12).

The Feynman diagrams for the dressed photonic Green's function, $\bar{P}_{k'\to k}(\omega) = \langle C_k \frac{1}{\omega - \mathcal{H} + i\delta} C^\dagger_{k'} \rangle_{\rm v}$, are shown in Fig. C.1(d). With the help of this diagram, $\bar{P}_{k'\to k}(\omega)$ is obtained as

$$\bar{P}_{k'\to k}(\omega) = \bar{P}^{(0)}_{k'\to k}(\omega) + \bar{P}^{(2)}_{k'\to k}(\omega)\,, \tag{C.11}$$

where

$$\bar{P}^{(0)}_{k'\to k}(\omega) = P_{k'\to k}(\omega) = \delta(k-k')Q(\omega-k)\,, \tag{C.12}$$

$$\begin{aligned}\bar{P}^{(2)}_{k'\to k}(\omega) &= \int dq'dq P_{k'\to q'}(\omega) g_{q'}\bar{A}(\omega) g^*_q P_{q\to k}(\omega) \\ &= g^2\eta^*(k')\eta(k)Q(\omega-k')\bar{A}(\omega)Q(\omega-k)\,.\end{aligned} \tag{C.13}$$

C.1.2. *Space representation*

Substituting Eq. (C.11) into Eq. (C.4), the one-photon propagator in the real-space representation is given by

$$G_{r'\to r}(t) = G^{(0)}_{r'\to r}(t) + G^{(2)}_{r'\to r}(t)\,, \tag{C.14}$$

where

$$G^{(0)}_{r'\to r}(t) = \delta(r-r'-t) - \kappa\theta(r'+t-r)e^{i\tilde{\omega}_{\rm c}(r-r'-t)}\,, \tag{C.15}$$

$$\begin{aligned}G^{(2)}_{r'\to r}(t) = \kappa\theta(r'+t-r)\Bigg[&e^{i\tilde{\omega}_{\rm c}(r-r'-t)} - \frac{\tilde{\omega}_2-\tilde{\omega}_{\rm c}}{\tilde{\omega}_2-\tilde{\omega}_1}e^{i\tilde{\omega}_1(r-r'-t)} \\ &- \frac{\tilde{\omega}_1-\tilde{\omega}_{\rm c}}{\tilde{\omega}_1-\tilde{\omega}_2}e^{i\tilde{\omega}_2(r-r'-t)}\Bigg]\,.\end{aligned} \tag{C.16}$$

The one-photon propagator is a function of a single argument, $r-r'-t$. The propagator vanishes in the region of $r > r'+t$ in agreement with the causality.

C.2. *Two-photon propagator*

Since the completeness relation in the two-photon space is given by $\hat{1} = 2^{-1}\int dr_1 dr_2 \tilde{b}^\dagger_{r_1}\tilde{b}^\dagger_{r_2}|0\rangle\langle 0|\tilde{b}_{r_1}\tilde{b}_{r_2}$, the two-photon propagator is identified as $2^{-1}\langle\tilde{b}_{r_1}\tilde{b}_{r_2}e^{-i\mathcal{H}t}\tilde{b}^\dagger_{r'_1}\tilde{b}^\dagger_{r'_2}\rangle_{\rm v}$. This quantity is composed of two types of terms. In the first (second) type, the photons initially located at r'_1 and r'_2 (r'_2 and r'_1) are scattered to r_1 and r_2, respectively. Both types yield the same output wavefunction, because the two-photon wavefunction is symmetric with respect to the interchange of the space coordinate, i.e. $\varphi(r'_1, r'_2) = \varphi(r'_2, r'_1)$. Therefore, we can regard only the first type as the two-photon propagator. The two-photon propagator is given by

$$G_{r'_1,r'_2\to r_1,r_2}(t) = \langle\tilde{b}_{r_1}\tilde{b}_{r_2}e^{-i\mathcal{H}t}\tilde{b}^\dagger_{r'_1}\tilde{b}^\dagger_{r'_2}\rangle_{\rm v}|_{r'_1\to r_1, r'_2\to r_2}\,. \tag{C.17}$$

Using Eq. (18), we can switch to the wavenumber representation:

$$\begin{aligned}G_{r'_1,r'_2\to r_1,r_2}(t) = \frac{i}{(2\pi)^3}\int d^2kd^2k'd\omega e^{i(k_1r_1+k_2r_2-k'_1r'_1-k'_2r'_2-\omega t)}\frac{\eta(k'_1)\eta(k'_2)}{\eta^*(k'_1)\eta^*(k'_2)} \\ \times\left\langle C_{k_1}C_{k_2}\frac{1}{\omega-\mathcal{H}+i\delta}C^\dagger_{k'_1}C^\dagger_{k'_2}\right\rangle_{\rm v}\Bigg|_{k'_1\to k_1, k'_2\to k_2}\,.\end{aligned} \tag{C.18}$$

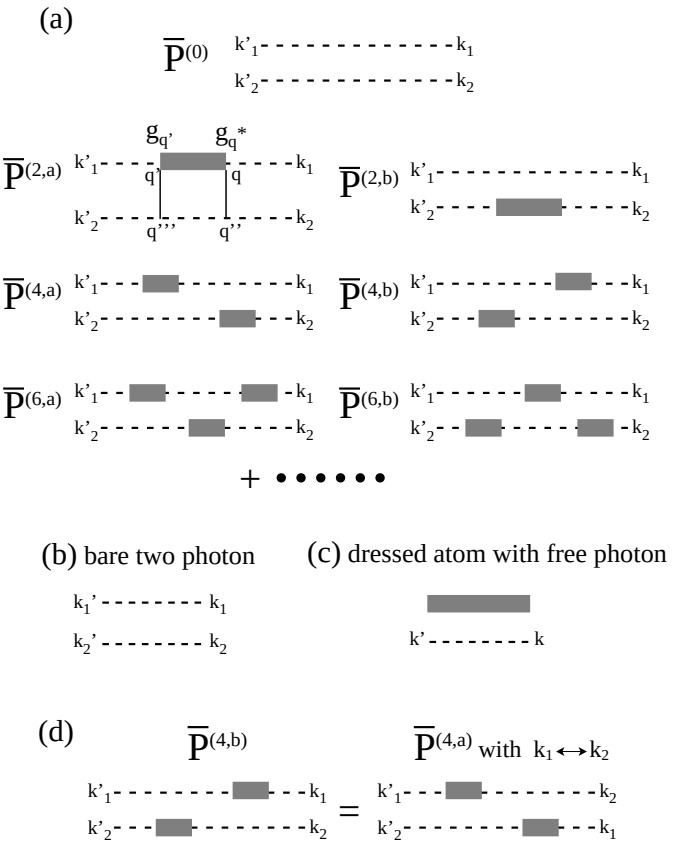

Fig. C.2. Feynman diagrams for the two-particle problem: (a) diagrams constituting the dressed two-photon Green's function, (b) bare two-photon Green's function, $P_{k_1'\to k_1,k_2'\to k_2}(\omega)$, (c) dressed atomic Green's function with a free photon, $\bar{A}_{k'\to k}(\omega)$, (d) equivalence between $\bar{P}^{(j,b)}$ and $\bar{P}^{(j,a)}$ with $k_1 \leftrightarrow k_2$.

C.2.1. *Green's function method*

We can apply the diagram technique also to two-quanta problems. The quantity to evaluate is the dressed two-photon Green's function,

$$\bar{P}_{k_1'\to k_1,k_2'\to k_2}(\omega) = \left\langle C_{k_1} C_{k_2} \frac{1}{\omega - \mathcal{H} + i\delta} C^\dagger_{k_1'} C^\dagger_{k_2'} \right\rangle_{\mathrm{v}} \Bigg|_{k_1'\to k_1,k_2'\to k_2} . \tag{C.19}$$

Noting that the atom cannot absorb two photons simultaneously, the low-order diagrams for this quantity are drawn in Fig. C.2(a). These diagrams are composed of two elementary components: the bare two-photon Green's function and the dressed atomic Green's function with a non-interacting photon, the diagrams of which are drawn in Figs. C.2 (b) and (c), respectively. They are given by

$$P_{k_1'\to k_1,k_2'\to k_2}(\omega) = \delta(k_1 - k_1')\delta(k_2 - k_2')Q(\omega - k_1 - k_2)\,, \tag{C.20}$$

$$\bar{A}_{k'\to k}(\omega) = \delta(k-k')\bar{A}(\omega-k)\,, \tag{C.21}$$

where $Q(\omega)$ and $\bar{A}(\omega)$ are defined by Eqs. (C.6) and (C.10). The dressed Green's function is given by

$$\bar{P}_{k_1'\to k_1,k_2'\to k_2}(\omega) = \bar{P}^{(0)} + \sum_{j=2,4,\ldots} (\bar{P}^{(j,a)} + \bar{P}^{(j,b)})\,, \tag{C.22}$$

where the arguments (k_1', k_2', k_1, k_2 and ω) are omitted in the right hand side. Figure C.2 shows that $\bar{P}^{(0)}$ is simply the bare two-photon Green's function given by Eq. (C.20). Furthermore, since the input wavenumbers k_1' and k_2' are interchangeable, $\bar{P}^{(j,b)}$ can be viewed as $\bar{P}^{(j,a)}$ with $k_1 \leftrightarrow k_2$, as illustrated in Fig. C.2(d). The higher-order terms take complicated forms, but they can be obtained systematically with the help of the diagram. For example, $\bar{P}^{(2,a)}$ is given by

$$\begin{aligned}\bar{P}^{(2,a)} &= \int d^4q P_{k_1'\to q',k_2'\to q'''}(\omega) g_{q'} \bar{A}_{q'''\to q''}(\omega) g_q^* P_{q\to k_1,q''\to k_2}(\omega) \\ &= g^2\eta^*(k_1')\eta(k_1)Q(\omega-k_1'-k_2')\bar{A}(\omega-k_2)Q(\omega-k_1-k_2) \\ &\quad\times \delta(k_2-k_2')\,. \end{aligned} \tag{C.23}$$

Similarly, $\bar{P}^{(4a)}$ and $\bar{P}^{(6a)}$ are given by

$$\begin{aligned}\bar{P}^{(4a)} &= g^4\eta^*(k_1')\eta^*(k_2')\eta(k_1)\eta(k_2)Q(\omega-k_1'-k_2')\bar{A}(\omega-k_2') \\ &\quad\times Q(\omega-k_1-k_2')\bar{A}(\omega-k_1)Q(\omega-k_1-k_2)\,, \end{aligned} \tag{C.24}$$

$$\begin{aligned}\bar{P}^{(6a)} &= g^6\eta^*(k_1')\eta^*(k_2')\eta(k_1)\eta(k_2)Q(\omega-k_1'-k_2')\bar{A}(\omega-k_2')\bar{A}(\omega-k_2) \\ &\quad\times Q(\omega-k_1-k_2)\int dq|\eta(q)|^2 Q(\omega-q-k_2')\bar{A}(\omega-q) \\ &\quad\times Q(\omega-q-k_2) \end{aligned} \tag{C.25}$$

$$\begin{aligned} &= g^6\eta^*(k_1')\eta^*(k_2')\eta(k_1)\eta(k_2)Q(\omega-k_1'-k_2')\bar{A}(\omega-k_2')\bar{A}(\omega-k_2) \\ &\quad\times Q(\omega-k_1-k_2)Q(\omega-\tilde{\omega}_{\rm c}-k_2')\bar{A}(\omega-\tilde{\omega}_{\rm c})Q(\omega-\tilde{\omega}_{\rm c}-k_2)\,. \end{aligned} \tag{C.26}$$

As observed in Eq. (C.25), for $P^{(j)}$ with $j \geq 6$, integrals over q's (inner photon wavenumber) remain. However, as in Eq. (C.26), such integrals can be evaluated simply by replacing q with $\tilde{\omega}_{\rm c}$.[g]

The infinite sum appearing in Eq. (C.22) can be obtained as

$$\bar{P}^{(\infty,a)} \equiv \bar{P}^{(6,a)} + \bar{P}^{(8,b)} + \bar{P}^{(10,a)} + \bar{P}^{(12,b)} + \cdots$$

[g]Typically, the integral over an inner wavenumber takes the following form: $\int dq|\eta(q)|^2 Q(\omega-q-z_1)\bar{A}(\omega-q)Q(\omega-q-z_2)$, where $\mathrm{Im}\, z_1, \mathrm{Im}\, z_2 \leq 0$. Because the integrand has only one pole (at $\tilde{\omega}_{\rm c}$) in the lower half-plane, we obtain the following formula,

$$\int dq|\eta(q)|^2 Q(\omega-q-z_1)\bar{A}(\omega-q)Q(\omega-q-z_2) = Q(\omega-\tilde{\omega}_{\rm c}-z_1)\bar{A}(\omega-\tilde{\omega}_{\rm c})Q(\omega-\tilde{\omega}_{\rm c}-z_2)\,.$$

By this formula, all integrals over the inner wavenumbers can be carried out.

$$= \bar{P}^{(6,a)} \times \frac{1}{1 - g^2 \bar{A}(\omega - \tilde{\omega}_{\rm c}) Q(\omega - 2\tilde{\omega}_{\rm c})}$$

$$= \bar{P}^{(6,a)} \times \frac{(\omega - \tilde{\omega}_{\rm c} - \tilde{\omega}_1)(\omega - \tilde{\omega}_{\rm c} - \tilde{\omega}_2)}{(\omega - \tilde{\nu}_1)(\omega - \tilde{\nu}_2)}\,, \tag{C.27}$$

where $\tilde{\nu}_1$ and $\tilde{\nu}_2$ are the complex eigenenergies with two quanta, defined by Eq. (13). The dressed two-photon Green's function is finally given by

$$\bar{P}(\omega) = \bar{P}^{(0)}(\omega) + \sum_{x=a,b} \{\bar{P}^{(2,x)}(\omega) + \bar{P}^{(4,x)}(\omega) + \bar{P}^{(\infty,x)}(\omega)\}\,. \tag{C.28}$$

C.2.2. *Space representation*

Combining Eqs. (C.18) and (C.28), the two-photon propagator in the real-space representation is given by

$$G_{r_1',r_2' \to r_1,r_2}(t) = G^{(0)} + \sum_{x=a,b} \{G^{(2,x)} + G^{(4,x)} + G^{(\infty,x)}\}\,, \tag{C.29}$$

where

$$G^{(0)}_{r_1',r_2' \to r_1,r_2}(t) = G^{(0)}_{r_1' \to r_1}(t) \times G^{(0)}_{r_2' \to r_2}(t)\,, \tag{C.30}$$

$$G^{(2,a)}_{r_1',r_2' \to r_1,r_2}(t) = G^{(2)}_{r_1' \to r_1}(t) \times G^{(0)}_{r_2' \to r_2}(t)\,, \tag{C.31}$$

$$G^{(4,a)}_{r_1',r_2' \to r_1,r_2}(t) = I^{(4)}(r_1 - r_2, r_1' - r_2', r_2 - r_1' - t)\,, \tag{C.32}$$

$$G^{(\infty,a)}_{r_1',r_2' \to r_1,r_2}(t) = I^{(\infty)}(r_2 - r_1, r_1' - r_2', r_1 - r_1' - t)\,, \tag{C.33}$$

and

$$I^{(4)}(x,y,z) = -\frac{ig^4\kappa^2}{8\pi^3} \int dk dk' d\omega \frac{e^{ikx + ik'y + i\omega z} J(k,k',\omega)}{\omega - k - k' + i\delta}\,, \tag{C.34}$$

$$I^{(\infty)}(x,y,z) = -\frac{ig^6\kappa^2}{8\pi^3} \int \frac{dk dk' d\omega\ e^{ikx + ik'y + i\omega z} J(k,k',\omega)(\omega - 2\tilde{\omega}_{\rm c})}{(\omega - k - \tilde{\omega}_{\rm c})(\omega - k' - \tilde{\omega}_{\rm c})(\omega - \tilde{\nu}_1)(\omega - \tilde{\nu}_2)}\,, \tag{C.35}$$

$$J(k,k',\omega) = \prod_{q=k,k'} \frac{1}{(q - \tilde{\omega}_{\rm c})(\omega - q - \tilde{\omega}_1)(\omega - q - \tilde{\omega}_2)}\,. \tag{C.36}$$

$G^{(j,b)}$ is obtained from $G^{(j,a)}$ by interchanging r_1 and r_2.

References

1. P. R. Berman (ed.), *Cavity Quantum Electrodynamics* (Academic Press, San Diego, 1994).
2. J. M. Raimond, M. Brune and S. Haroche, *Rev. Mod. Phys.* **73**, 565 (2001).
3. H. Mabuchi and A. C. Doherty, *Science* **298**, 1372 (2002).
4. G. Rempe, H. Walther and N. Klein, *Phys. Rev. Lett.* **58**, 353 (1987).

5. B. T. H. Varcoe, S. Brattke, M. Weidinger and H. Walther, *Nature* **403**, 743 (2000).
6. S. Brattke, B. T. H. Varcoe and H. Walther, *Phys. Rev. Lett.* **86**, 3534 (2001).
7. E. Hagley, X. Maitre, G. Nogues, C. Wunderlich, M. Brune, J. M. Raimond and S. Haroche, *Phys. Rev. Lett.* **79**, 1 (1997).
8. A. Rauschenbeutel, G. Nogues, S. Osnaghi, P. Bertet, M. Brune, J. M. Raimond and S. Haroche, *Science* **288**, 2024 (2000).
9. G. Nogues, A. Rauschenbeutel, S. Osnaghi, M. Brune, J. M. Raimond and S. Haroche, *Nature* **400**, 239 (1999).
10. P. W. H. Pinkse, T. Fischer, P. Maunz and G. Rempe, *Nature* **404**, 365 (2000).
11. C. J. Hood, T. W. Lynn, A. C. Doherty, A. S. Parkins and H. J. Kimble, *Science* **287**, 1447 (2000).
12. K. M. Birnbaum, A. Boca, R. Miller, A. D. Boozer, T. E. Northup and H. J. Kimble, *Nature* **436**, 87 (2005).
13. Y. R. Shen, *Principles of Nonlinear Optics* (Wiley-Interscience, New York, 1984).
14. N. Bloembergen, *Nonlinear Optics* (World Scientific, Singapore, 1996).
15. R. W. Boyd, *Nonlinear Optics* (Academic Press, Boston, 2002).
16. Q. A. Turchette, R. J. Thompson and H. J. Kimble, *Appl. Phys. B* **60**, S1 (1995).
17. Q. A. Turchette, C. J. Hood, W. Lange, H. Mabuchi and H. J. Kimble, *Phys. Rev. Lett.* **75**, 4710 (1995).
18. M. A. Nielsen and I. L. Chuang, *Quantum Computation and Quantum Information* (Cambridge University Press, Cambridge, 2000).
19. A. Aspect, J. Dalibard and G. Roger, *Phys. Rev. Lett.* **49**, 1804 (1982).
20. P. G. Kwiat, K. Mattle, H. Weinfurter, A. Zeilinger, A. V. Sergienko and Y. Shih, *Phys. Rev. Lett.* **75**, 4337 (1995).
21. O. Benson, C. Santori, M. Pelton and Y. Yamamoto, *Phys. Rev. Lett.* **84**, 2513 (2000).
22. S. Takeuchi, *Opt. Lett.* **26**, 843 (2001).
23. C. Santori, D. Fattal, J. Vukovi, G. S. Solomon and Y. Yamamoto, *Nature* **419**, 594 (2002).
24. K. Edamatsu, G. Oohata, R. Shimizu and T. Itoh, *Nature* **431**, 167 (2004).
25. M. O. Scully and M. S. Zubairy, *Quantum Optics* (Cambridge University Press, Cambridge, 1997).
26. P. Meystre and M. Sargent III, *Elements of Quantum Optics*, 3rd edn. (Springer-Verlag, Berlin, 1998).
27. C. W. Gardiner and P. Zoller, *Quantum Noise : A Handbook of Markovian and Non-Markovian Quantum Stochastic Methods with Applications to Quantum Optics*, 3rd edn. (Springer-Verlag, Berlin, 2004).
28. D. F. Walls and G. J. Milburn, *Quantum Optics*, 2nd edn. (Springer-Verlag, Berlin, 2006).
29. B. Yurke and D. Stoler, *Phys. Rev. Lett.* **57**, 13 (1986).
30. G. J. Milburn, *Phys. Rev. Lett.* **62**, 2124 (1989).
31. W. J. Munro, K. Nemoto and T. Spiller, *New J. Phys.* **7**, 137 (2005).
32. K. Kojima, H. F. Hofmann, S. Takeuchi and K. Sasaki, *Phys. Rev. A* **68**, 013803 (2003).
33. H. F. Hofmann, K. Kojima, S. Takeuchi and K. Sasaki, *Phys. Rev. A* **68**, 043813 (2003).
34. K. Koshino and H. Ishihara, *Phys. Rev. A* **70**, 013806 (2004).
35. K. Koshino and H. Ishihara, *Phys. Rev. Lett.* **93**, 173601 (2004).
36. K. Koshino and H. Ishihara, *Phys. Rev. A* **71**, 063818 (2005).
37. E. T. Jaynes and F. W. Cummings, *Proc. IEEE* **51**, 89 (1963).
38. H. F. Hofmann and G. Mahler, *Quantum Semiclassic. Opt.* **7**, 489 (1995).

39. G. D. Boyd and J. P. Gordon, *Bell Syst. Tech. J.* **40**, 489 (1961).
40. H. Kogelnik and T. Li, *Proc. IEEE* **54**, 1312 (1966).
41. K. Koshino and A. Shimizu, *Phys. Rep.* **412**, 191 (2005).
42. U. Fano, *Phys. Rev.* **124**, 1866 (1961).
43. K. Koshino, *Phys. Rev. A* **73**, 053814 (2006).
44. H. Haug and S. W. Koch, *Quantum Theory of the Optical and Electronic Properties of Semiconductors* (World Scientific, Singapore, 1988).
45. H. F. Hofmann, K. Kojima, S. Takeuchi and K. Sasaki, *J. Opt. B: Quantum Semiclassical Opt.* **5**, 218 (2003).
46. H. Oka, S. Takeuchi and K. Sasaki, *Phys. Rev. A* **72**, 013816 (2005).
47. E. Fredkin and T. Toffoli, *Int. J. Theor. Phys.* **21**, 219 (1982).
48. C. C. Gerry and P. L. Knight, *Introductory Quantum Optics* (Cambridge University Press, Cambridge, 2005).
49. C. K. Hong, Z. Y. Ou and L. Mandel, *Phys. Rev. Lett.* **59**, 2044 (1987).